

Rift- and subduction-related crustal sequences in the Jinshajiang ophiolitic mélangé, SW China: Insights into the eastern Paleo-Tethys

Wen-Jun Hu^{1,2}, Hong Zhong^{1,3,*}, Wei-Guang Zhu¹, and Zhong-Jie Bai¹

¹STATE KEY LABORATORY OF ORE DEPOSIT GEOCHEMISTRY, INSTITUTE OF GEOCHEMISTRY, CHINESE ACADEMY OF SCIENCES, GUIYANG 550081, CHINA

²DEPARTMENT OF EARTH SCIENCES, THE UNIVERSITY OF HONG KONG, HONG KONG, CHINA

³COLLEGE OF EARTH AND PLANETARY SCIENCES, UNIVERSITY OF CHINESE ACADEMY OF SCIENCES, BEIJING 100049, CHINA

ABSTRACT

The Paleozoic Jinshajiang ophiolitic mélangé in southwest China marks an important branch ocean (i.e., the Jinshajiang Ocean) of the Paleo-Tethys. Basic-intermediate rocks are widespread features in the mélangé; their formation age is well known, but the petrogenesis has not been well studied, which means that the evolutionary history of the Jinshajiang Ocean is not well constrained. To understand the nature of the mélangé and the ocean, we present a set of elemental and isotopic data from two typical crustal sequences in two areas of the Jinshajiang ophiolitic mélangé, Zhiyong and Baimaxueshan. The basalts in the ca. 343 Ma Zhiyong crustal sequence show mid-ocean-ridge basalt-like geochemical compositions with Nb/La ratios of 0.98–1.15 and $\epsilon_{\text{Nd}}(t)$ values of +6.5 to +7.7, indicating that the basalts formed in the spreading ridge of the ocean. In contrast, the 283 Ma Baimaxueshan crustal sequence consists of gabbros and basaltic-andesitic lavas, which have an arc affinity with Nb/La ratios of 0.54–0.67 and $\epsilon_{\text{Nd}}(t)$ values of +5.1 to +6.5. The geochemical differences were not caused by crustal assimilation but reflect mantle metasomatism by fluids dehydrated from the subducting slab. Therefore, we propose that the Zhiyong and Baimaxueshan crustal sequences formed in seafloor spreading and subduction settings, which were related to the opening and closure of the ocean, respectively.

LITHOSPHERE, v. 11; no. 6; p. 821–833 | Published online 22 October 2019

<https://doi.org/10.1130/L1091.1>


INTRODUCTION

Ophiolites are fragments of ancient oceanic lithosphere, including oceanic crust and the underlying upper mantle, which were generated in a variety of tectonic settings and then emplaced onto a continental margin. Specifically, ophiolites can be generated at almost every stage of the whole life cycle of oceanic basins, from continental rifting to seafloor spreading, ocean closure, and final continental collision (Dilek and Furnes, 2011, 2014; Pearce, 2014). Therefore, identification of the formation environment of ophiolites is crucial to reconstruct the plate history. Oceanic crust in ophiolites, including lavas and plutonic rocks, is generated by a combination of multiple processes, from mantle metasomatism to partial melting to magma fractionation; therefore, the crustal sequence carries an important record about the igneous processes that occurred during the

formation of the oceanic lithosphere, which in turn can help to reveal the tectonic origin of ophiolites and provide insights into the evolution of oceanic basins (e.g., Miyashiro, 1973; Pearce and Robinson, 2010; Pearce, 2014).

The Paleo-Tethys Ocean was a Paleozoic ocean separating the Gondwana and Laurasia supercontinents; it started to open in the Devonian and closed in the Late Triassic (Şengör, 1987; Stampfli and Borel, 2002; Metcalfe, 2013). Paleo-Tethys-related suture zones containing ophiolitic mélanges are now preserved in the Sanjiang area, southwest China (Fig. 1; Metcalfe, 1996, 2006, 2011, 2013; Mo et al., 1998; Zhong, 1998; Deng et al., 2014; Wang et al., 2018). The Changning-Menglian suture marks the collisional closure of the main Paleo-Tethys Ocean, which separated the Baoshan-Sibumasu block to the west from the Qamdo-Simao block to the east (e.g., Metcalfe, 1996; Mo et al., 1998; Zhong, 1998; Jian et al., 2008, 2009a, 2009b). The Ailaoshan and the Jinshajiang sutures resulted from closure of a branch ocean or a back-arc basin (Zhong, 1998; Wang et al., 2000a). A typical ophiolite

in the Ailaoshan suture zone, the Shuanggou ophiolite is analogous to those formed at slow-spreading ridges or at continental margins, with crustal sequences similar to normal mid-ocean-ridge-basalts (N-MORB; Yumul et al., 2008; Hu et al., 2015; Lai et al., 2014a). The Jinshajiang suture has been proposed to be connected with the Ailaoshan suture. However, previous studies on the ophiolite in the Jinshajiang suture mainly focused on geochronology (e.g., Jian et al., 2008, 2009b) but paid less attention to petrogenesis and geochemistry, especially to the basic-intermediate crustal sequence. As a consequence, we have limited knowledge of the Jinshajiang ophiolite and the lithosphere of the Jinshajiang Ocean, for example, whether the Jinshajiang Ocean developed from a back-arc basin due to the subduction of the main Paleo-Tethys Ocean plate (Metcalfe, 1996, 2006, 2011, 2013; Mo et al., 1998; Zhong, 1998; Jian et al., 2009a, 2009b; Fan et al., 2010). The relation between the Jinshajiang suture and the Ailaoshan suture also needs to be checked regarding the geochemical difference between crustal sequences in the Ailaoshan and

Hong Zhong  <http://orcid.org/0000-0002-5871-2380>

*Corresponding author: zhonghong@vip.gyig.ac.cn

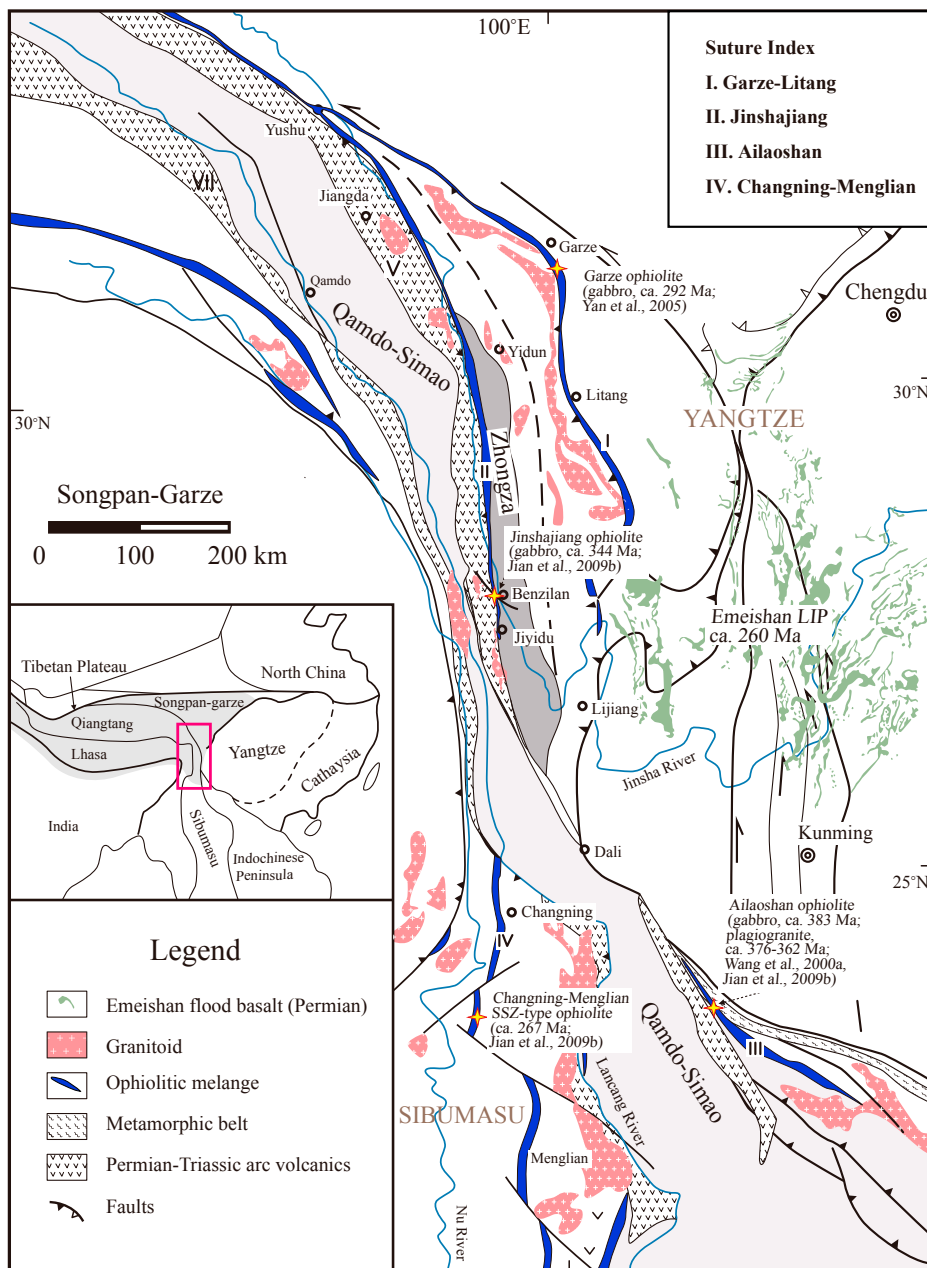


Figure 1. Index map of the major Paleo-Tethys suture zones (ophiolitic belts) and tectonic units in the Sanjiang area, southwest China (after Zi et al., 2012b). SSZ—suprasubduction zone; LIP—large igneous province.

Jinshajiang ophiolites (e.g., Jian et al., 2009a, 2009b; Hu et al., 2015; Lai et al., 2014a). To help resolve some of these issues, we carried out detailed elemental and isotopic studies of the crustal sequences (e.g., gabbros and basalts) of the Jinshajiang ophiolite and integrated the results with previous geochronological studies (e.g., Jian et al., 2008, 2009b). Our aims were (1) to constrain the mantle source and genesis of these rocks and (2) to clarify the tectonic history of the ocean.

GEOLOGICAL BACKGROUND AND SAMPLE PETROGRAPHY

The N-S–striking Jinshajiang ophiolite-bearing orogenic belt is located in the eastern part of the Sanjiang area, southwest China (Fig. 1; Mo et al., 1998; Zhong, 1998; Wang et al., 2000a; Jian et al., 2009a, 2009b; Wang et al., 2018). It separates the Qamdo-Simao block to the west and the Zhongza block to the east. The basement of the Qamdo-Simao block consists of

the high-grade Damenglong and Chongshan complexes (Zhong, 1998; Wang et al., 2000a, 2000b, 2006). The Damenglong complex contains greenschists, metavolcanics, graywacke, iron formation, and amphibolite with granitoid intrusions (the Lincang batholith; Yang et al., 1994), and the Chongshan complex is composed of gneiss, amphibolite, and graywacke intercalated with phyllitic basic-intermediate metavolcanics and medium- to thick-bedded, fine- to medium-grained marble (Wei et al., 1984; Wu et al., 1984). Metasediments of the Lower Ordovician section, as the oldest exposed sedimentary rocks in the Qamdo-Simao block, are characterized by slates, phyllites, quartzites, and meta-limestones that are analogous to those in the Lower Ordovician of the Yangtze block. The Middle Devonian section unconformably overlies the Lower Ordovician and is characterized by basal conglomerates and shallow-marine sediments. Moreover, the Carboniferous and the Permian strata are mainly composed of shallow-marine, paralic, and continental sediments with coal measures in places, while the Lower–Middle Triassic strata consist of shallow-marine clastics and carbonates (Bureau of Geology and Mineral Resources of Yunnan Province [BGM-RYP], 1990; Metcalfe, 2006). The variation in sedimentary facies indicates that the Qamdo-Simao block had become part of the Yangtze block before Middle Devonian time (Wang et al., 2000a, 2006; Zhong, 1998) but was later separated from the Yangtze block, thereby leading to the birth of the Jinshajiang Ocean.

In the Zhongza block, a massive basaltic flow with compositions comparable to the Emeishan flood basalt disconformably overlies the Lower Permian section, and it is overlain by the Upper Permian sedimentary rocks (Bureau of Geology and Mineral Resources of Sichuan Province [BGMRS], 1991). The Lower Permian section contains massive limestone-bearing purple pelitic bands and fossils such as *Sumatrina longissima*, *Neoschwagerina cheni*, *Chusenella schwagerinae formis*, *Pseudodoliolina tubaensis*, and coral. The Lower Permian section in the Zhongza block is comparable with that in the Yangtze block. However, the Upper Permian section in the Zhongza block is characterized by more submarine sedimentary deposits, including sandstone, siltstone, and limestone and black shale interbedded with coal, relative to that in the Yangtze block. This feature indicates that the Zhongza-Zhongdian block was a part of the Yangtze block but was then separated from it in the Permian in response to the opening of the Garze-Litang Ocean in the late Paleozoic (Li et al., 2010).

The Jinshajiang orogenic belt has four parts, from east to west, including a foreland fold-and-thrust belt, an ophiolite mélange zone, a

collision-related volcano-sedimentary zone, and a continental margin arc zone (Fig. 2; Zi et al., 2013). The foreland thrust zone is made up of a series of west-verging structural slices, including Devonian–Permian turbidites, carbonates, and basalts. These rocks were developed on the passive margin of the Yangtze block (Leloup et al., 1995; Li et al., 2002). The ophiolite mélangé zone marks the ancient lithosphere of the Jinshajiang Ocean and is thought to connect with the Ailaoshan ophiolite mélangé zone to the south (e.g., Wang et al., 2000a). The collisional volcano-sedimentary zone was built along the margin of the Qamdo-Simao block, and it is characterized by an association of bimodal (felsic and mafic) volcanic rocks with the Triassic turbidites and clastic sequences, suggesting an abyssal or bathyal environment (Mou and Wang, 2000; Yu et al., 2000; Tan, 2002). The continental margin arc is located at the eastern margin of the Qamdo-Simao block. It was generated by westward subduction of the Jinshajiang oceanic plate in the Permian (Zi et al., 2012a, 2012b, 2012c, 2013).

The Jinshajiang ophiolites consist of a number of blocks that occur within a N–S–striking tectonic mélangé zone along the Jinsha River over a distance of hundreds of kilometers (Fig. 1). The ophiolite is composed of dismembered peridotite, cumulate rocks, and volcanic rocks with intercalated limestone and radiolarian cherts (Mo et al., 1998; Wang et al., 2000a). These rocks are blocks or olistoliths enclosed in a turbiditic sequence of Middle Triassic age unconformably covered by Late Triassic continental red sandstone (Faure et al., 2016). Mantle peridotites are dominated by harzburgites with minor dunites, which have been largely serpentinized. Large-size (1 km across) peridotites are exposed as irregular veins or strip bodies, while small-size (<100 m across) peridotites occur as dismembered lenticular bodies. Cumulate ultramafic rocks including harzburgites, dunites, and pyroxenites only occur in the Xumai area; these rocks are separated from the mantle rocks by faults (Mo et al., 1998). The typical rock assemblage in the cumulate rocks is represented by an association of layered gabbros and anorthites (Wang, 1985; Mo et al., 1998; Jian et al., 2008). Pillow lavas range from basalt to andesite in composition and are widely distributed in the mélangé; the pillow structure can be up to 3 m in width with developed chilled rims, as well as radiated fractures, indicating they were produced by submarine eruption processes (Wang, 1985). This study carried out sampling in two typical areas of the Jinshajiang ophiolitic mélangé, i.e., the Baimaxueshan area and the Zhiyong area. In the Baimaxueshan area, serpentinized harzburgites are scattered within

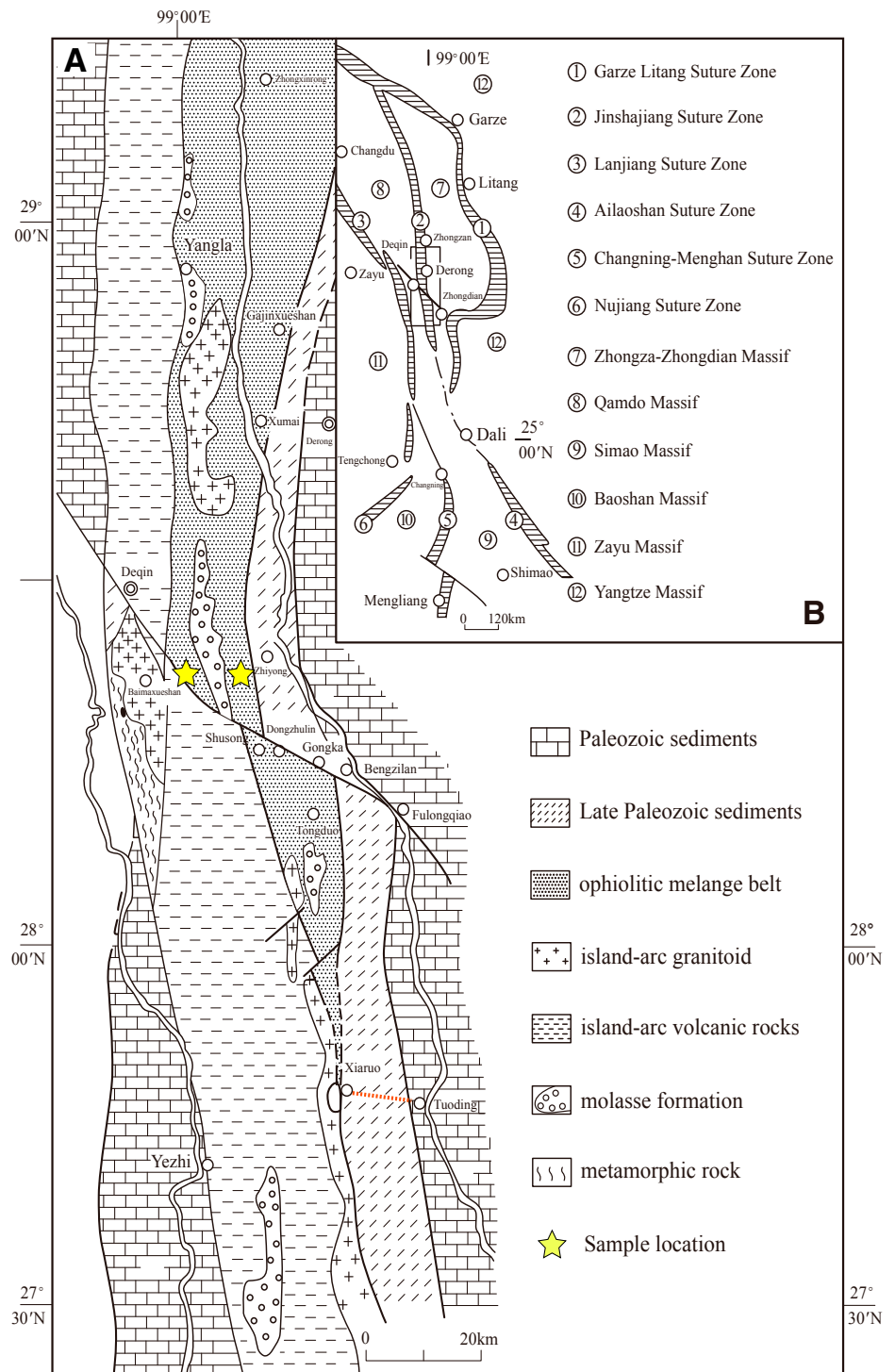


Figure 2. Geological sketch maps (A) of the Jinshajiang orogenic belt and (B) of the Sanjiang area (after Sun and Jian, 2004). Sample location is exhibited as yellow stars. The red dashed line shows the location of the Xiaruo-Tuoding area.

sheared sandy silt, while the crustal sequence is mainly composed of layered gabbros and pillow lavas. The age of this crustal sequence has been constrained as 285–282 Ma based on zircon U–Pb dating from the gabbros (Jian et al., 2008).

Gabbro samples exhibit a typical gabbroic/ophiolitic texture and consist of subhedral-euhedral plagioclase (~65 modal%) and xenomorphic-subhedral granular clinopyroxene (~30 modal%; Fig. 3A). The lavas are basalts and andesites

with a typical porphyritic texture. Phenocrysts of plagioclase outnumber those of clinopyroxene (Fig. 3B). The groundmass of the andesites consists of small microlites of feldspar embedded in glass (Fig. 3C). In the Zhiyong area, the crustal sequence is composed of pillow lava and layered amphibole gabbros with ages of 343.5 ± 2.7 Ma (Jian et al., 2008, 2009b). The Zhiyong lavas are typical amygdaloidal basalts with porphyritic textures consisting of plagioclase phenocrysts in an intergranular groundmass (Fig. 3D).

ANALYTICAL METHODS

Whole-rock major oxides were measured with a ME-XRF 06 spectrometer with <5% relative standard deviation at the ALS Laboratory, Guangzhou, China. Trace elements were analyzed with an inductively coupled plasma–mass spectrometer (ICP-MS) with an analytical precision better than 5% at the State Key Laboratory of Ore Deposit Geochemistry, Chinese Academy of Sciences (SKLOGD), Guiyang, China. The detailed procedure for basic–intermediate rocks was described by Qi et al. (2000).

Whole rock Sr–Nd isotopes were analyzed on a Thermo Fisher Triton thermal ionization mass spectrometer (TIMS) at SKLOGD. The analytical procedure was as follows: 0.11 g of rock powder was added in Teflon capsules with mixed HF + HNO₃ + HClO₄. After complete dissolution of the sample, the solution was dried, and 6 mol/L HCl was then added and evaporated to dryness (twice). The residue was dissolved with 1.5 mL HCl at 2.5 mol/L. After centrifugal separation, 1 mL of the supernatant was passed through a cation exchange resin (AG50W × 12), and 5 mol/L HCl was used to elute Sr. Then, 6 mol/L HCl was used to elute rare earth elements (REEs), and the solution was dried. Next, 0.1 mol/L HCl was passed through an anion exchange resin (P507), and 0.2 mol/L HCl was added to elute Nd. Mass fractionation corrections for Sr and Nd isotopic ratios were based on values of ⁸⁶Sr/⁸⁸Sr = 0.1194 and ¹⁴⁶Nd/¹⁴⁴Nd = 0.7219, respectively. Measured values were ⁸⁷Sr/⁸⁶Sr = 0.710250 ± 7 (2σ) for NBS987, and ¹⁴³Nd/¹⁴⁴Nd = 0.512612 ± 8 (2σ) and ¹⁴³Nd/¹⁴⁴Nd = 0.512104 ± 5 (2σ) for the BCR-2 and JNdi-1 standards, respectively.

ANALYTICAL RESULTS

Major-oxide and trace-element data are listed in Table 1. The Zhiyong lavas are basaltic in composition, with SiO₂ from 48.48% to 51.42% and MgO from 6.28% to 7.58% (Fig. 4A). With decreasing MgO, Al₂O₃ decreases from 16.83% to 13.95% (Fig. 4B), while Fe₂O₃ increases from 7.18% to 10.76% (Fig. 4C). In the Baimaxueshan

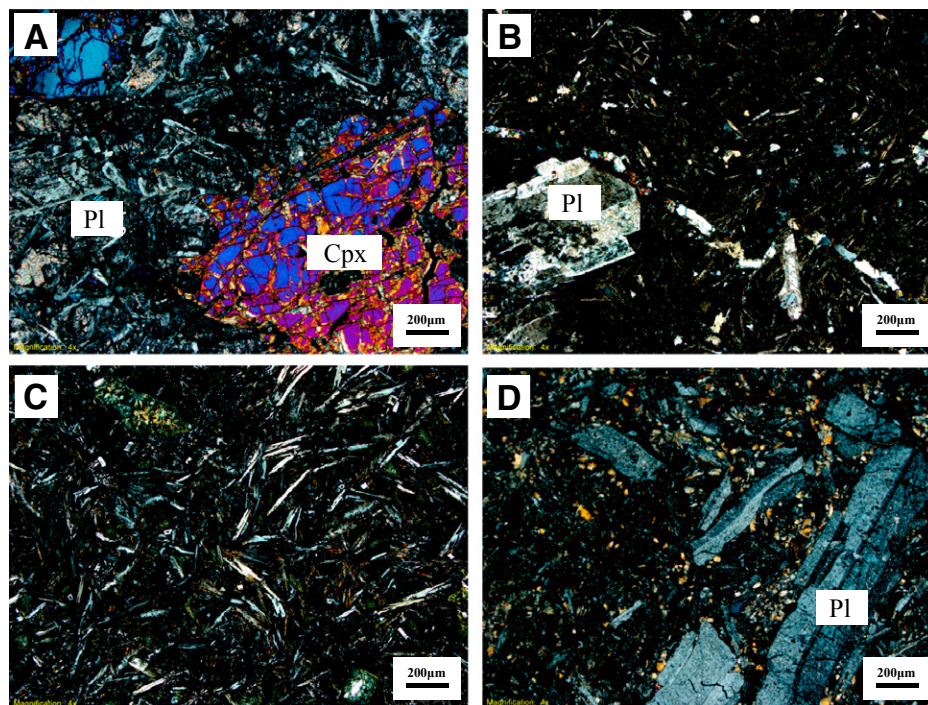


Figure 3. Photomicrographs of (A) Baimaxueshan gabbro (plane-polarized light), showing accumulation of plagioclase (Pl) and clinopyroxene (Cpx); (B) Baimaxueshan basalt with typical porphyritic texture; (C) Baimaxueshan andesite with groundmasses of hyalopilitic texture; and (D) Zhiyong basalt consisting of porphyritic texture with intergranular groundmass and plagioclase (Pl) phenocrysts.

crustal sequence, the gabbros have SiO₂ from 47.10% to 53.08% and MgO from 4.37% to 8.90%, while the lavas have SiO₂ contents ranging from 46.56% to 58.48% and lower MgO contents from 2.74% to 4.91%, which show positive correlations with Al₂O₃ (12.19%–14.62%) and Fe₂O₃ (9.22%–11.93%; Figs. 4B and 4C).

The Zhiyong basalts display flat or slightly light (L) REE–enriched REE patterns with low (La/Yb)_N (1.10–1.95) and (Sm/Yb)_N ratios (1.23–1.36) and variable REE concentrations (35.9–91.5 ppm; Fig. 5A). In the primitive mantle–normalized trace-element diagram, the Zhiyong basalts do not exhibit any depletions in high field strength elements (HFSEs; e.g., Nb and Ta; Fig. 5B). In comparison, the Baimaxueshan lavas are characterized by flat or slightly LREE-enriched patterns (Fig. 5C), with low (La/Yb)_N (1.00–1.78) and (Sm/Yb)_N ratios (1.01–1.27) and relatively constant REE concentrations (50.46–63.22 ppm), but in a primitive mantle–normalized spider diagram, they show considerable depletion in HFSEs (e.g., Nb, Ta) and variable enrichment in Pb (Fig. 5D). The gabbros exhibit trace-element features (Figs. 5E and 5F) similar to the Baimaxueshan lavas. In particular, the lavas show variable depletions of Sr, while the gabbros exhibit positive Sr anomalies, indicating that Sr concentrations were mainly controlled by the crystallization of plagioclase.

Isotope data are listed in Table 2. The initial isotope compositions were calculated for ages of 343 Ma and 283 Ma for the Zhiyong and Baimaxueshan rocks, respectively (Jian et al., 2008, 2009b). The Zhiyong lavas without any Nb depletion tend to have slightly higher $\epsilon_{Nd}(t)$ values (6.5–7.1) but lower (⁸⁷Sr/⁸⁶Sr)_i ratios (0.704052–0.705452) than those of the Baimaxueshan lavas and gabbros, which have $\epsilon_{Nd}(t)$ values from +5.1 to +6.5 and (⁸⁷Sr/⁸⁶Sr)_i values from 0.704531 to 0.707347 (Fig. 6).

DISCUSSION

MORB Preserved in the 343 Ma Zhiyong Crustal Sequence

The Zhiyong crustal sequence contains trace-element patterns (e.g., flat REE chondrite-normalized patterns; Fig. 5) and isotope compositions ($\epsilon_{Nd}[t]$ from +6.5 to +7.1; Fig. 6) that have strong affinities to enriched (E) MORB. The negative correlations between Fe₂O₃ and MgO suggest that the fractionation of clinopyroxene was limited (Fig. 4C), whereas the overall positive correlations between Al₂O₃ and MgO reflect the fractionation of plagioclase and olivine (Fig. 4B). Scandium (Sc) is a useful indicator for the fractionation of clinopyroxene because it is highly compatible with clinopyroxene but incompatible

TABLE 1. MAJOR- AND TRACE-ELEMENT COMPOSITIONS OF LAVAS FROM THE JINSHAJIANG OPHIOLITE

Sample	Zhiyong lava					Baimaxueshan lava						Baimaxueshan gabbro						
	DQ1120	DQ1105	DQ1121	DQ0903	DQ0904	DQ1117	DQ1114	DQ0905	DQ1118	DQ1116	DQ0906	DQ1109	DQ1115	09DQ02	DQ0907	DQ1111	DQ1119	09DQ03
Major elements determined by XRF (wt%)																		
SiO ₂	48.48	49.13	50.13	51.32	51.42	46.56	52.38	54.57	53.74	55.27	58.48	47.02	47.88	49.18	48.86	50.93	53.08	47.10
Al ₂ O ₃	15.44	16.83	15.45	13.95	14.44	12.54	14.62	13.24	12.19	13.00	12.56	16.25	19.68	18.86	16.77	17.47	14.91	18.78
Fe ₂ O ₃	10.27	7.18	9.36	10.57	10.76	11.01	11.32	11.93	9.22	9.59	11.52	8.10	5.62	7.36	10.37	9.44	8.32	8.04
MgO	7.12	7.58	7.26	6.65	6.28	3.57	4.91	3.62	3.20	2.74	3.62	5.76	6.75	6.70	5.88	4.37	5.59	8.90
CaO	8.53	11.35	8.17	9.62	8.37	10.39	4.97	6.69	8.80	7.02	4.51	7.65	10.04	7.83	6.23	4.88	6.15	6.49
Na ₂ O	3.36	2.73	3.25	3.14	3.91	3.94	4.69	4.34	4.10	5.47	5.66	4.77	2.94	3.49	3.65	4.62	3.26	2.14
K ₂ O	0.62	0.38	0.58	0.19	0.43	0.03	0.09	0.31	0.20	0.05	0.03	0.05	1.50	1.58	0.59	0.86	1.15	2.35
TiO ₂	1.44	0.88	1.38	1.52	1.42	1.46	1.51	1.53	1.28	1.33	1.61	1.07	0.63	0.73	1.21	1.28	0.96	0.74
P ₂ O ₅	0.17	0.10	0.17	0.17	0.14	0.17	0.16	0.16	0.14	0.15	0.17	0.15	0.08	0.09	0.14	0.21	0.14	0.06
MnO	0.17	0.11	0.16	0.16	0.15	0.15	0.15	0.18	0.15	0.15	0.19	0.16	0.09	0.10	0.12	0.17	0.15	0.11
LOI	3.34	3.00	3.41	2.69	2.68	8.58	5.25	3.45	5.56	3.62	1.68	8.04	4.41	4.11	6.43	5.84	4.47	5.33
Total	98.94	99.27	99.32	99.96	100.00	98.40	100.05	100.01	98.58	98.39	100.03	99.05	99.62	100.04	100.25	100.07	98.18	100.04
Trace elements determined by ICP-MS (ppm)																		
Cs	1.87	3.13	1.58	1.59	3.03	1.17	1.63	0.38	0.40	0.51	0.85		24.97	1.54	9.20	6.57	5.63	2.45
Rb	20.2	9.8	15.9	6.5	13.5	0.7	0.9	4.5	3.0	0.8	0.6	0.8	59.5	8.5	22.9	32.7	46.9	10.7
Ba	240	90	305	99.3	149	24.0	59.5	43.9	39.5	16.6	23.0	26	654.1	59.9	195	309	517	141
Sr	218	240	186	302	239	36.9	187	114	63.4	34.3	30.9	110	410	262	244	351	210	426
Pb	1.52	1.17	8.52	1.42	0.75	1.39	0.98	0.76	1.10	2.70	2.40	3.39	2.31	4.64	1.58	5.67	3.13	12.12
Th	1.00	0.47	1.34	1.60	1.15	0.91	0.78	0.67	0.64	0.89	0.90	0.70	0.41	1.51	0.74	1.49	1.19	1.21
U	0.33	0.18	0.36	0.41	0.37	0.25	0.22	0.24	0.23	0.21	0.26	0.17	0.11	0.40	0.21	0.38	0.33	0.32
Zr	99.0	61.4	101	146	102	117	111	91.1	94.3	113	109	111	40	150	60.3	110	136	127
Hf	2.73	1.67	2.83	3.82	2.80	3.12	3.01	2.64	2.62	3.03	2.79	2.74	1.12	3.61	1.73	2.97	3.63	3.13
Ta	0.44	0.39	0.59	0.84	0.54	0.48	0.26	0.22	0.20	0.29	0.28	0.40	0.20	0.38	0.19	0.36	0.27	0.33
Y	33.4	22.1	31.8	42.1	31.6	34.0	37.6	28.7	32.6	33.5	28.5	26.8	13.9	33.1	19.8	33.9	36.3	28.3
Nb	7.31	3.23	9.73	13.30	8.02	4.37	3.56	3.14	3.09	4.02	4.21	3.90	2.23	5.56	2.69	4.59	4.30	4.68
Sc	30.6	26.5	29.1	38.3	32.7	26.0	32.0	30.3	27.7	27.9	29.2	30.3	28.0	37.5	27.2	22.6	26.8	34.8
Cr	203	417	206	271	191	3.12	6.27	11.6	0.59	2.38	21.7	236	293	252	162	64.6	113	240
Ni	86.2	110.3	75.6	115	78.2	8.31	12.1	11.1	9.84	7.6	11.3	192.2	59.9	68.2	99.0	33.2	45.7	65.9
Co	41.4	35.5	37.0	49.1	36.9	33.3	35.4	27.6	32.2	23.4	24.8	32.0	26.3	34.6	31.2	26.0	28.7	29.5
V	258	190	239	317	250	335	330	262	297	351	227	60	170	256	166	206	191	241
Ga	14.4	12.5	14.1	18.2	14.9	20.1	16.2	13.3	14.1	18.7	13.0	88.1	13.8	18.4	12.6	17.1	15.8	17.1
Zn	106	68	100	124	98.9	100	103	89.3	97.7	149	113		47	116	77.5	107	77.6	115
Cu	53.0	53.2	46.8	65.3	46.3	53.6	50.3	42.3	51.1	54.6	54.0		41.0	72.8	58.0	48.0	49.6	53.5
La	7.45	3.53	8.78	11.6	7.68	7.06	6.50	5.46	4.45	7.37	7.42	7.70	3.29	9.49	4.61	7.86	7.66	7.95
Ce	16.4	8.67	18.6	25.2	17.0	15.6	14.4	12.5	11.0	16.2	16.6	16.8	6.9	24.0	10.4	18.8	17.4	19.4
Pr	2.35	1.35	2.70	3.58	2.45	2.28	2.16	1.84	1.70	2.28	2.25	2.32	0.99	3.46	1.54	2.74	2.49	2.86
Nd	11.4	6.64	12.6	18.2	12.2	11.0	10.6	9.63	8.78	10.9	10.8	10.7	4.8	16.7	7.58	13.2	11.9	13.4
Sm	3.54	2.33	3.71	5.37	3.87	3.49	3.44	3.32	3.04	3.30	3.41	3.13	1.47	4.72	2.50	3.96	3.67	3.94
Eu	1.25	0.84	1.22	1.78	1.31	1.29	1.22	1.05	1.00	1.22	1.16	1.02	0.68	1.65	0.96	1.31	1.18	1.44
Gd	3.85	2.47	4.00	5.71	4.26	3.86	4.03	3.57	3.36	3.67	3.89	3.27	1.65	5.21	2.66	4.36	4.16	4.13
Tb	0.75	0.50	0.79	1.15	0.89	0.72	0.82	0.77	0.73	0.74	0.76	0.65	0.32	1.01	0.55	0.83	0.82	0.83
Dy	5.32	3.71	5.43	7.18	5.44	5.55	5.84	4.96	5.26	5.31	5.03	4.57	2.41	5.79	3.47	5.84	5.87	5.16
Ho	1.19	0.79	1.19	1.74	1.28	1.16	1.30	1.17	1.18	1.16	1.18	0.92	0.52	1.32	0.82	1.26	1.30	1.16
Er	3.40	2.35	3.36	4.37	3.46	3.51	3.95	3.39	3.43	3.32	3.24	2.83	1.49	3.63	2.09	3.58	3.97	3.13
Tm	0.44	0.29	0.47	0.67	0.54	0.46	0.52	0.48	0.47	0.44	0.46	0.37	0.19	0.57	0.32	0.48	0.52	0.46
Yb	3.16	2.09	3.25	4.36	3.38	3.28	3.77	3.11	3.20	3.17	2.99	2.61	1.33	3.23	2.12	3.34	3.72	3.05
Lu	0.49	0.34	0.50	0.64	0.48	0.52	0.58	0.44	0.52	0.48	0.42	0.39	0.19	0.49	0.31	0.51	0.58	0.46

Note: XRF—X-ray fluorescence; LOI—loss on ignition; ICP-MS—inductively coupled plasma—mass spectrometry.

Figure 4. Diagrams of MgO vs. selected elements, illustrating different fractionation sequences and types of the Zhiyong and Baimaxueshan crustal sequences. Red dots—Zhiyong lavas; blue dots—Baimaxueshan lavas; blue squares—Baimaxueshan gabbros. Normal arc lavas range from basaltic andesites (BA) to andesites (A), dacites (D), and rhyolites (R) (the BADR series). B—basalt; BON—boninite; HMA—high-magnesium andesite.

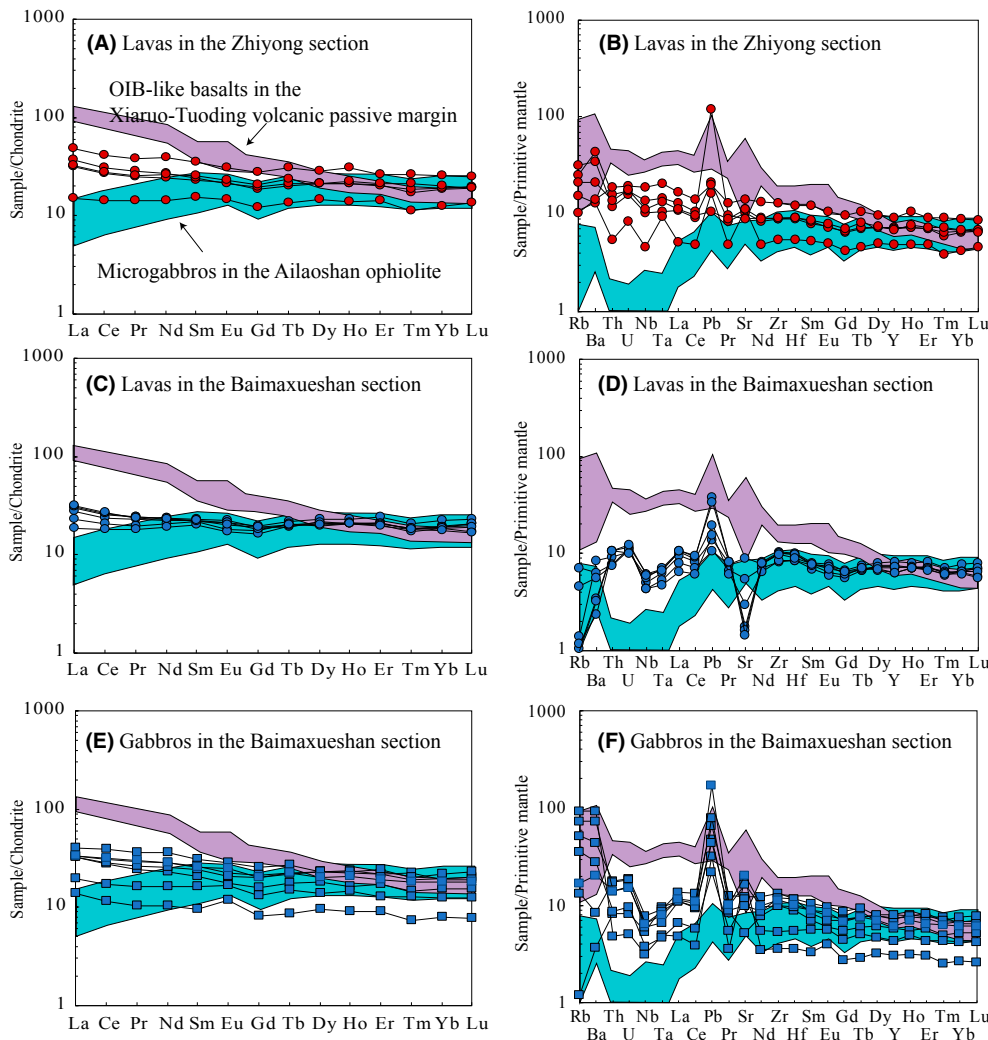
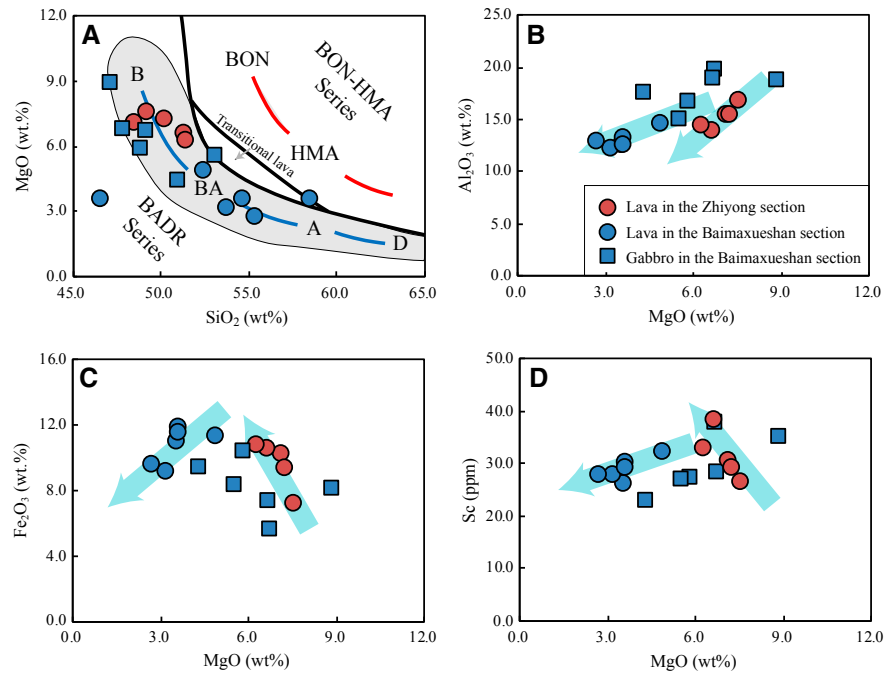


Figure 5. (A) Chondrite-normalized rare earth element (REE) diagrams and (B) primitive mantle-normalized incompatible element distribution spidergrams of the Zhiyong lavas. (C) Chondrite-normalized REE diagrams and (D) primitive mantle-normalized incompatible element distribution spidergrams of the Baimaxueshan lavas. (E) Chondrite-normalized REE diagrams and (F) primitive mantle-normalized incompatible element distribution spidergrams of the Baimaxueshan gabbros. The normalization values are from Sun and McDonough (1989). The green and purple areas represent compositions of diabases of the Ailaoshan ophiolite (Hu et al., 2015) and oceanic-island basalt (OIB)-like basalts in the volcanic rift margin (Xiao et al., 2008), respectively.

TABLE 2. Sr AND Nd ISOTOPIC COMPOSITIONS OF LAVAS FROM THE JINSHAJIANG OPHIOLITE

Sample no.	Rb (ppm)	Sr (ppm)	⁸⁷ Rb/ ⁸⁶ Sr	⁸⁷ Sr/ ⁸⁶ Sr	Error(2σ)	(⁸⁷ Sr/ ⁸⁶ Sr) _i	Sm (ppm)	Nd (ppm)	¹⁴⁷ Sm/ ¹⁴⁴ Nd	¹⁴³ Nd/ ¹⁴⁴ Nd	Error(2σ)	(¹⁴³ Nd/ ¹⁴⁴ Nd) _i	ε _{Nd} (t)
Zhiyong lava (343 Ma)													
DQ1120	20.24	218	0.2682	0.706361	20	0.705051	3.54	11.35	0.1877	0.512958	4	0.512536	6.6
DQ1105	9.81	240	0.1185	0.705499	27	0.704920	2.33	6.64	0.2108	0.513064	11	0.512591	7.7
DQ1121	15.89	186	0.2475	0.705262	10	0.704054	3.71	12.56	0.1780	0.512933	4	0.512534	6.6
DQ0903	6.48	302	0.0621	0.705115	18	0.704811	5.37	18.20	0.1775	0.512928	4	0.512530	6.5
DQ0904	13.50	239	0.1634	0.706251	31	0.705453	3.87	12.20	0.1909	0.512988	15	0.512559	7.1
Baimaxueshan lava (283 Ma)													
DQ1117	0.68	37	0.0532	0.707561	11	0.707347	3.49	11.00	0.1909	0.512895	6	0.512541	5.2
DQ1114	0.89	187	0.0138	0.704880	12	0.704824	3.44	10.56	0.1958	0.512969	8	0.512606	6.5
DQ0905	4.52	114	0.1147	0.704993	15	0.704531	3.32	9.63	0.2075	0.512972	14	0.512588	6.1
DQ1118	2.96	63	0.1349	0.706101	5	0.705558	3.04	8.78	0.2086	0.512963	6	0.512577	5.9
DQ1116	0.76	34	0.0637	0.705886	7	0.705630	3.30	10.94	0.1816	0.512898	4	0.512562	5.6
Baimaxueshan gabbro (283 Ma)													
DQ1115	59.47	410	0.4199	0.708109	6	0.706418	1.47	4.77	0.1848	0.512878	4	0.512536	5.1
09DQ02	8.46	262	0.0934	0.707685	17	0.707309	4.72	16.70	0.1701	0.512907	17	0.512592	6.2
DQ1119	46.89	210	0.6447	0.708076	11	0.705480	3.67	11.88	0.1857	0.512923	5	0.512579	6.0

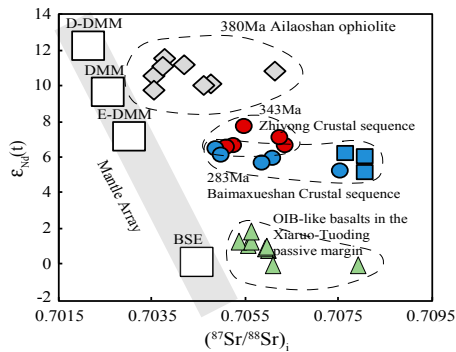


Figure 6. Sr-Nd isotope compositions of lavas and gabbros in the Jinshajiang ophiolite. Diabases of the Ailaoshan ophiolite are also presented as gray diamonds in the diagram (Xu and Castillo, 2004; Hu et al., 2015). Oceanic-island basalt (OIB)-like basalts in the volcanic rift margin are presented as green triangles (Xiao et al., 2008). Other symbols are the same as in Figure 4. DDM—depleted mid-ocean-ridge basalt (MORB) mantle; D-DMM—depleted-DMM; E-DMM—enriched-DMM; BSE—bulk silicate earth.

with plagioclase and olivine (Niu et al., 2002). Similar to the correlation between Fe_2O_3 and MgO , Sc steadily increases with decreasing MgO (Fig. 4D), implying the absence of clinopyroxene during fractionation. Thus, according to the correlation between the major elements, the fractionation crystallization sequence was dominated by olivine and plagioclase with negligible clinopyroxene fractionation. The fractionation sequence is similar to that of MORB, which takes place in a low-pressure anhydrous environment, because petrological experiments illustrate that decompression can expand the liquidus crystallization fields of plagioclase and olivine and suppress the field of clinopyroxene (O'Hara, 1968; Bender et al., 1978; Presnall et al., 1978, 1979; Grove et al., 1982; Fujii and Bougault, 1983), and a high

magmatic water content, which is associated with subduction, can expand the stability field of clinopyroxene at the expense of plagioclase (Gaetani et al., 1993).

All these features support the interpretation that the Zhiyong basalts formed by upwelling of the asthenosphere beneath a spreading ridge. Compared with the diabases from the Ailaoshan ophiolite (Xu and Castillo, 2004; Hu et al., 2015), which represent the oceanic crust of the Ailaoshan Ocean, the Zhiyong basalts show not only a relatively enrichment in LREEs, but also slightly lower Nd isotope ratios (Fig. 6). Because there is no evidence of involvement of a slab component or crustal assimilation (e.g., Nb-Ta depletion), the data illustrate that the asthenosphere beneath the ocean was similar to that of enriched depleted MORB mantle (E-DMM) as proposed by Workman and Hart (2005), providing evidence of heterogeneity in the upper mantle of the Paleo-Tethys. The melting of the source was in the low-pressure spinel field, as reflected by the flat REE pattern of the lavas. Following the batch melting equation of Shaw (1970), the Zhiyong lavas were generated by moderate-degree (~10%) partial melting (Fig. 7).

Oceanic Subduction Recorded by the 283 Ma Baimaxueshan Crustal Sequence

In comparison with the Zhiyong lavas, the lavas and gabbros in the 283 Ma Baimaxueshan crustal sequence are characterized by significant depletions in HFSEs (e.g., Nb) with relatively lower $\epsilon_{\text{Nd}}(t)$ values and higher Sr isotope values (Figs. 5 and 6). These geochemical features clearly indicate the involvement of sediments in the genesis of the Baimaxueshan crustal sequence, which was either related to metasomatism in the mantle source or crustal contamination during magma fractionation

(Jahn et al., 1999; Fan et al., 2010; Bezdard et al., 2014). To discriminate between these two processes, the relations between indices of magma fractionation (e.g., SiO_2) and whole-rock trace elements are often used (e.g., Fan et al., 2010; Bezdard et al., 2014). As shown in Figure 8, the subchondritic Nb/La ratios and $\epsilon_{\text{Nd}}(t)$ values remain constant irrespective of the variation of the SiO_2 contents, implying that these values were not controlled by magma fractionation. In other words, these compositional features of the Baimaxueshan crustal sequence were unrelated to crustal contamination processes, so they were more likely a result of mantle metasomatism.

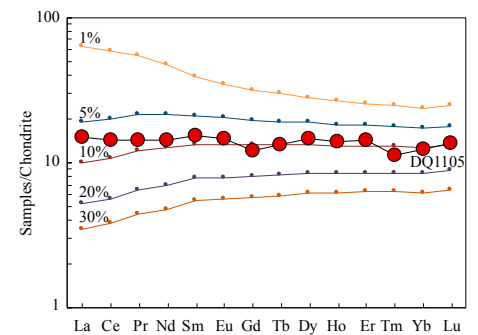


Figure 7. Chondrite-normalized rare earth element (REE) diagrams for comparison between modeled melts and the Zhiyong lava. DQ1105, with high MgO contents and low REE contents, was selected for modeling. Partition coefficients are from McKenzie and O'Nions (1991, 1995). Undepleted/flat heavy REE profiles suggest that the melting process was in the spinel field. The modes (olivine: 57%; orthopyroxene: 28%; clinopyroxene: 13%; spinel: 11%) and chemical compositions are from Workman and Hart (2005). Melt modes (olivine: -6%; orthopyroxene: 28%; clinopyroxene: 67%; spinel: 11%) during partial melting of spinel-bearing peridotites are from Workman and Hart (2005).

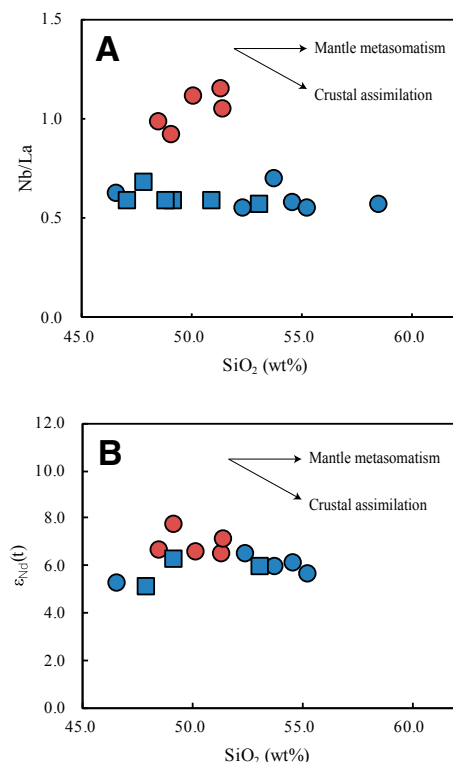


Figure 8. (A) SiO_2 vs. Nb/La . (B) SiO_2 vs. $\epsilon_{\text{Nd}}(t)$. The constant Nb/La and $\epsilon_{\text{Nd}}(t)$ values irrespective of the variation of SiO_2 contents illustrates the fact that the geochemical composition of the Baimaxueshan crustal sequence was controlled by mantle metasomatism rather than by crustal assimilation. Symbols are the same as in Figure 4.

Located in the foreland thrust zone, the Xiaruo-Tuoding area contains a complete stratigraphic sequence from the Devonian to Permian, which developed on the volcanic-rifted passive margin of the Yangtze block (Feng et al., 1999; Sun and Jian, 2004; Xiao et al., 2008). The sequence records detailed information about the evolution of the ocean. In the recovered stratigraphic sequence, the Upper Devonian sequence is composed of gray marlite, crystalline limestone, and black mudstone, indicating a neritic-bathyal setting. Moreover, the Lower Carboniferous consists of gray phyllite and quartz schist intercalated with bathyal fossiliferous crystalline limestone (Feng et al., 1999). Basalts in the Lower Carboniferous show affinities with the oceanic-island basalt (OIB; Zhang et al., 1996). The Upper Carboniferous consists of carbonate breccia and turbidite limestone with synsedimentary slump and scour structures. The Upper Carboniferous also is composed of basic volcanic breccia with OIB-like geochemical compositions (Fig. 5; Xiao et al., 2008). The lithology of the Lower Permian section is complex, including turbidite sandstone, pebbled sand shale, conglomerate, carbonate-slipping

rock, breccia, turbidite limestone, crystalline limestone, braided limestone, and basalt. Furthermore, the characteristics of the Upper Permian sedimentary combination indicate that the area was located in a continental slope to shallow sea environment. Based on the characteristics of the stratigraphic sequence, Sun and Jian (2004) proposed that the Jinshajiang Ocean was a mature ocean in the Carboniferous after continental breakup in the Late Devonian, and it started to close in the Permian.

Therefore, the previous discussion indicates that the Baimaxueshan crustal sequence likely formed in an arc system during the closure stage of the Jinshajiang Ocean, when the mantle source had been metasomatized by fluids or melts released from the slab. We further propose that this crustal sequence formed in an oceanic arc rather than a continental arc, where crustal assimilation is very common. The oceanic arc setting is also consistent with previous studies on the 283 Ma tonalite in the Jiyudu area of the Jinshajiang mélange (Zi et al., 2012b). In general, the development of oceanic subduction can be separated into three stages (Ishizuka et al., 2011; Reagan et al., 2010; Whattam and Stern, 2011): (1) When oceanic lithosphere starts to sink, the asthenosphere will upwell into the overlying void and further melt due to decompression, leading to the formation of forearc basalts, which are chemically similar to MORB (Reagan et al., 2010). (2) As subduction continues, the depleted mantle will further melt due to the slab input. Magma in this stage is generally boninitic, with high SiO_2 and MgO contents, enriched in the fluid mobile trace elements (e.g., Rb, Ba, K, LREEs) but depleted in fluid immobile elements (e.g., heavy [H] REEs and HFSEs). The REE patterns of boninites are usually U-shaped, reflecting middle (M) REE depletion relative to LREEs and HREEs (Crawford et al., 1989; Tatsumi and Maruyama, 1989; Taylor et al., 1994; Falloon and Danyushevsky, 2000). (3) The “normal” arc lavas then form as the subduction zone steps into the mature stage with a change to flux melting in counterflowing mantle. The magmas in different stages of subduction form different series. On the one hand, boninite is a special rock type in a subduction zone, with >53 wt% SiO_2 , $\text{TiO}_2 < 0.5$ wt%, and $\text{Mg\#} > 0.65$ (Crawford et al., 1989). Boninites may be the primary magma of many high-magnesium andesites (HMA) in an arc system. On the other hand, normal arc lavas range from basaltic andesites (BA) to andesites (A), dacites (D), and rhyolites (R) (the BADR series). From Figure 4A, it is clear that the Baimaxueshan lavas are clearly distinguished from the HMA series, but they vary within the range of the BADR series. Therefore, the 283 Ma

Baimaxueshan crustal sequence was not related to boninites, because it has an affinity with normal arc lavas. The available evidence suggests that the Baimaxueshan crustal sequence marks a mature oceanic arc in the Jinshajiang Ocean.

In subduction zones, sediments and altered oceanic crust (AOC) of the subducting slab contribute to the overlying mantle wedge, which eventually leads to chemical variations of the lavas (Nielsen and Marschall, 2017). These crustal materials may be transported through melts and fluids that are released from the sediments and AOC of the slab (Brenan et al., 1995; Kessel et al., 2005; Plank, 2005). The effects of melt and fluid metasomatism are different. Fluids from dehydration of a slab are enriched in the fluid mobile elements and depleted in fluid immobile elements, while melts from melting of a slab are enriched in both fluid mobile and fluid immobile elements. For example, a slab fluid has lower Nd concentrations and in turn has minor effects on the Nd isotopic compositions of the mantle source overlying the subducted slab. In contrast, slab melts have higher Nd concentrations with radiogenic Nd isotopic compositions, and, consequently, metasomatism by slab melts can significantly change the Nd isotopic composition of the upper mantle (Peng et al., 2008). Therefore, still-unradiogenic Nd isotope ratios in the Baimaxueshan crustal sequence favor a slab-derived fluid modification process. Both Th and Nd are not mobile during slab dehydration (Brenan et al., 1995); therefore, the input of a slab fluid may not change the Th/Nd ratio of the source and of the lavas. In contrast, sediments usually have higher Th/Nd ratios than the mantle, and it has been experimentally determined that a sediment melt has much higher Th/Nd ratios (Johnson and Plank, 2000); therefore, the addition of a high-Th/Nd slab melt will greatly change the composition of the source and the lavas. As to the Baimaxueshan lavas, in comparison to the variation of Sr/Nd ratios and Nd isotope ratios, the Th/Nd ratios are very low with limited variations (Fig. 9). This suggests that the predominate metasomatizing agent was a fluid dehydrated from a slab rather than a slab melt. We used two end-member mixing to estimate the nature and the proportion of involved fluid in the mantle source (Li et al., 2012). Our quantitative calculations indicate that the source of the Baimaxueshan crustal sequences had been modified by addition of $<5\%$ sediment-derived fluid (Fig. 10).

Comparison between the Jinshajiang and Ailaoshan Sutures

The Ailaoshan suture zone is located to the southeast of the Jinshajiang suture zone (Fig. 1),

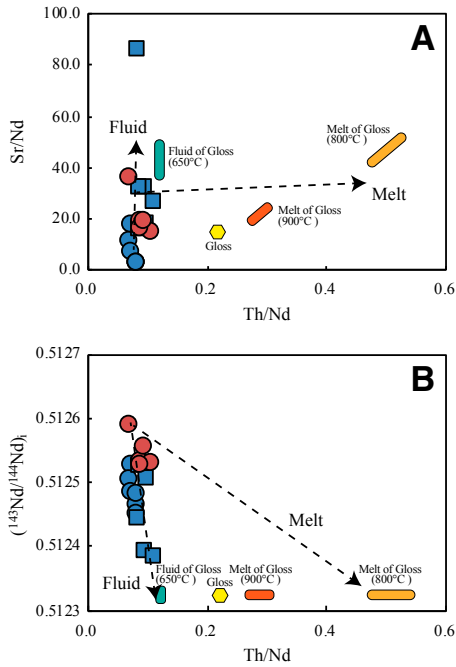


Figure 9. Variations of (A) Sr/Nd and (B) $^{143}\text{Nd}/^{144}\text{Nd}$ with Th/Nd, demonstrating different effects of fluid- and melt-mantle metasomatism. Fluid and melt compositions of GLOSS (“global subducting sediment,” after Plank and Langmuir, 1998) were calculated by Woelki et al. (2018) using the experimentally determined partition coefficients of Johnson and Plank (2000).

and it has lithological assemblages and deformation-metamorphic history comparable to the Jinshajiang suture zone. Therefore, it has been widely accepted that the two sutures are contiguous and represent the same ocean basin, i.e.,

the Jinshajiang-Ailaoshan Ocean (Wang et al., 2000a). This point is important for reconstructing the paleogeography of the Paleo-Tethys. Nevertheless, by integrating our data with relevant information in the literature, several differences between the two sutures should be taken into consideration.

First of all, the Ailaoshan and Jinshajiang sutures are ~300 km apart (Fig. 1). The ophiolite in the Ailaoshan suture zone is characterized by the dominance of lherzolite in the mantle sequence, minor portions of the mafic rocks, and absence of sheeted dikes. These features are similar to those of lithosphere at slow-spreading ridges or at continental margins (Pamić et al., 2002; Schaltegger et al., 2002; Montanini et al., 2008). Jian et al. (2009b) reported Late Devonian ages for a diabase (382.9 ± 3.9 Ma) and a plagiogranite sample (375.9 ± 4.2 Ma), indicating that the oceanic crust preserved in the Ailaoshan ophiolite is older than the oceanic crust preserved in the Jinshajiang ophiolite. These temporal and spatial differences thus indicate diachronous opening of the Jinshajiang-Ailaoshan Ocean (Zhong, 1998; Wang et al., 2000a).

Second, high-grade metamorphic rock assemblages in the Ailaoshan suture are considered to be representative of the continent-ocean transition zone, and they are in fault contact with the Yangtze block to the east and an olistostrome to the west (Jian et al., 2009a, 2009b). These geological features are characteristic of a nonvolcanic rifted margin (Froitzheim and Manatschal, 1996; Hopper et al., 2004), and on these grounds, Jian et al. (2009b) proposed a detached-rifting system, which caused the

thinning of the lithosphere and the seafloor spreading of the Ailaoshan segment. In contrast, the Jinshajiang ophiolitic mélange is associated with a volcanic-rifted margin, as indicated by the stratigraphic sequence in the Xiaruo-Tuoding area. Mafic volcanic rocks interbedded in Carboniferous and Permian sedimentary rocks exhibit OIB-like geochemical compositions with high LREE and HFSE contents (Fig. 5; Zhang et al., 1996; Xiao et al., 2008) and Nd isotope compositions ($\epsilon_{\text{Nd}}[t] = -1.43$ to $+1.9$) close to primitive mantle (Fig. 6; Xiao et al., 2008). It should be noted that these geochemical and isotopic signatures are very similar to those of the Emeishan flood basalts, which are located to the east of the Jinshajiang suture zone (Fig. 1; Xiao et al., 2008).

Last, the diabases in the Ailaoshan ophiolite, which represent ancient oceanic crust, have N-MORB-like trace-element characteristics with LREE-depleted patterns and positive $\epsilon_{\text{Nd}}(t)$ values ($+9.7$ to $+11.6$; Figs. 5 and 6; Hu et al., 2015). In contrast, the Zhiyong crustal sequence, which represents oceanic crust in the spreading ridge of the Jinshajiang Ocean, is characterized by E-MORB-like compositions with higher LREE/HREE ratios and lower $\epsilon_{\text{Nd}}(t)$ values. The presence of E-MORB at mid-ocean ridges has long been considered as evidence for plume-ridge interactions (Schilling, 1973; Schilling et al., 1983; Le Roux et al., 2002; Cushman et al., 2004). Together with the presence of the volcanic-rift margin containing OIB-like basalts, we propose that, unlike the Ailaoshan segment, the genesis of the oceanic crust in the Jinshajiang segment of the Ailaoshan-Jinshajiang Ocean was affected by a long-lived Paleo-Tethys

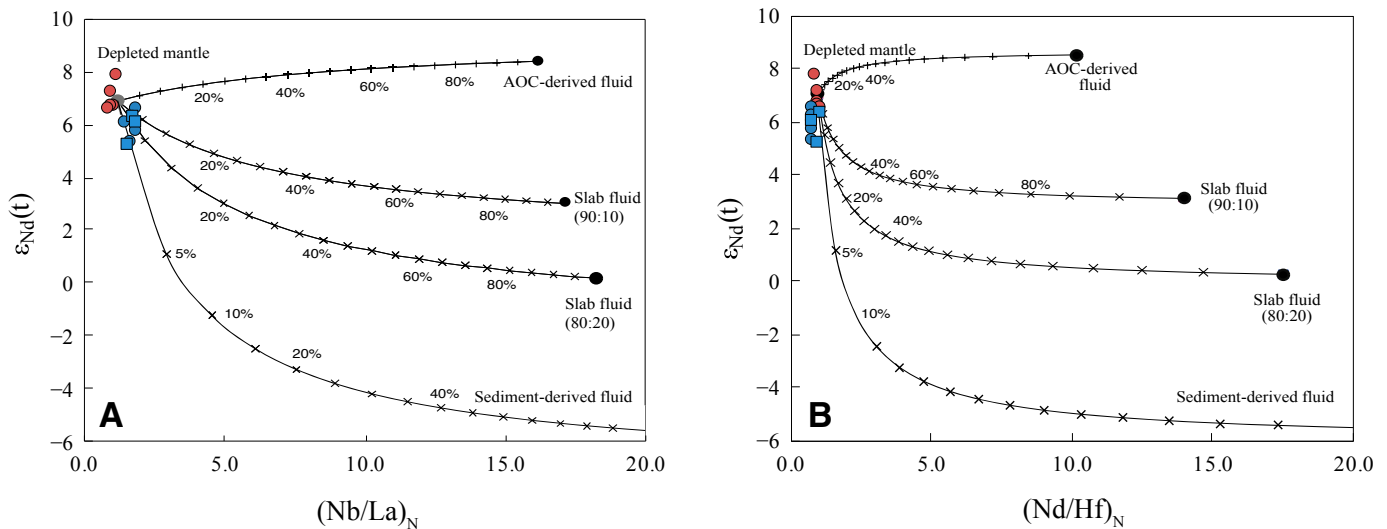


Figure 10. (A) $\epsilon_{\text{Nd}}(t)$ vs. primitive mantle-normalized La/Nb and (B) $\epsilon_{\text{Nd}}(t)$ vs. Nd/Hf ratios for the Zhiyong and Baimaxueshan crustal sequences. The primitive mantle values are from Sun and McDonough (1989). The compositions of mantle and slab components are from the compilation of Li et al. (2012). AOC—altered oceanic crust.

mantle plume, since the stage of continent rifting. The Paleo-Tethys mantle plume might have subsequently produced the ca. 260 Ma Emeishan flood basalt (Xiao et al., 2008).

Evolution of the Jinshajiang-Ailaoshan Ocean

The tectonic environment of the Jinshajiang-Ailaoshan Ocean has been hotly debated (Fan et al., 2010; Jian et al., 2009a, 2009b). To date, two different tectonic settings have been proposed: (1) a subduction-related back-arc basin (Metcalf, 1996, 2006; Wang et al., 2000a) and (2) a subduction-unrelated branch ocean with a slow spreading velocity (Mo et al., 1998; Zhong, 1998). In this contribution, we propose that the first model of subduction-related back-arc basin is inappropriate. First, in terms of regional geology, the requisite associated arc related to subduction of the main Paleo-Tethys Ocean and the opening of the Jinshajiang-Ailaoshan Ocean has not been located or reported. Second, as proposed in this study, the 343 Ma Zhiyong crustal sequence represents the oceanic crust of the Jinshajiang Ocean, while the oceanic crust in the Ailaoshan ophiolite is ~383 m.y. old. Additionally, the oldest igneous rocks in the Jinshajiang mélange are the low-Ti continental flood basalt (CFB) xenoliths (ca. 443–401 Ma), which show enriched LREE and high Ba, Sr, Nb, and Ta concentrations, indicating the onset of crustal extension (Jian et al., 2009b). These ages are much older than the age of subduction of the main Tethys Ocean, which was in the Early Permian, as suggested by the geochronological data of Jian et al. (2009b). For example, Alaskan-type mafic-ultramafic complexes and arc rocks formed by subduction of the main Paleo-Tethys plate yield zircon ages of 306.2 ± 4.6 Ma for a tonalite, 301.0 ± 2.9 Ma for a microgabbro, 297.1 ± 2.0 Ma for a plagioclase hornblende, and 281.3 ± 1.7 Ma for a diabase (Jian et al., 2009b). Third, the oceanic crust of the Jinshajiang-Ailaoshan Ocean, represented by the 343 Ma Zhiyong crustal sequence and the 383 Ma Ailaoshan diabbases, lacks evidence of involvement of slab components during its genesis. Based on this evidence, we therefore propose that the Jinshajiang-Ailaoshan Ocean represents a branch ocean rather than a back-arc basin in the Paleo-Tethys. The evolution of the Jinshajiang-Ailaoshan Ocean is presented in Figure 11.

In the Early Devonian, the Qamdo-Simao block started to rift from the Yangtze block (Fig. 11A). The rifted western Yangtze margin consisted of two segments, the Ailaoshan segment in the south and the Jinshajiang segment in the north (Wang et al., 2000a). The

Ailaoshan segment was a nonvolcanic rift margin (Jian et al., 2009a, 2009b). Juxtaposition of lower-crustal and mantle rocks in the high-grade Ailaoshan metamorphic complex indicates that detachment faulting caused the removal of crust and consequent exhumation of mantle (Jian et al., 2009a, 2009b; Hu et al., 2015). Crustal extension of the Jinshajiang segment might have taken place at 443–401 Ma, as recorded by the low-Ti CFB xenoliths in the Jinshajiang ophiolite (Jian et al., 2009a, 2009b). OIB-like basalts preserved in the Carboniferous–Permian strata postdate the rifting of the Jinshajiang segment, indicating that the rift margin was distal to the mantle plume in the Early Devonian.

Seafloor spreading in the Ailaoshan segment occurred at ca. 380 Ma (Fig. 11B), leading to the generation of the Ailaoshan ophiolite (Jian et al., 2009a, 2009b). The lithological characteristics of the Ailaoshan ophiolite, including the dominance of lherzolite in the mantle sequence, minor portions of mafic rocks, and absence of the sheeted dikes, is similar to those formed at slow spreading ridges (Pamić et al., 2002; Schaltegger et al., 2002; Montanini et al., 2008). Oceanic crust in the Ailaoshan segment is similar to N-MORB (Hu et al., 2015). As a result, the Ailaoshan segment has been interpreted as a slow-spreading oceanic basin (Zhang et al., 1995; Zhong, 1998; Jian 2009a, 2009b). In contrast, the Jinshajiang segment was still at the rifting stage at that time. At 340 Ma, deep melt from the mantle plume–established rift systems transformed the established Jinshajiang rift system into a volcanic rift margin and formed the OIB-like basalts preserved in the volcanic rift margin. This led to the seafloor spreading in the Jinshajiang segment (Fig. 11C). Meanwhile, the asthenosphere in the Jinshajiang segment was influenced by the plume, and therefore could produce oceanic crust comparable to E-MORB.

After reaching its maximum expansion in the late Carboniferous, the Jinshajiang-Ailaoshan Ocean started to close by westward subduction under the Qamdo-Simao block in the Early Permian. Oceanic subduction took place almost simultaneously in the Jinshajiang and Ailaoshan segments (Fig. 11D), as documented by the 280 Ma Baimaxueshan crustal sequence in the Jinshajiang ophiolitic mélange and the 287 Ma Wusu basalt in the Western Ailaoshan volcanic belts (Fan et al., 2010). Subduction of the Jinshajiang oceanic lithosphere promoted the Zhongza block to separate from the Yangtze block, resulting in opening of the Garze-Litang Ocean along the western Yangtze during Early Permian time (Li et al., 2010). The closure of the ocean also caused the change in the relative position between the mantle plume and the Yangtze block, which promoted formation of the ca. 260

Ma Emeishan flood basalt to the east of the Jinshajiang Ocean (Fig. 11D; Xiao et al., 2008). The consumption of the ocean transitioned to collision between the Qamdo-Simao block and the Yangtze block in the Late Permian–Early Triassic, with formation of associated syncollisional granitoid plutons close to the Baimaxueshan crustal sequence (Zi et al., 2012a) and within the Western Ailaoshan volcanic belts (Fig. 11E; Lai et al., 2014b). Meanwhile, crust formed either in the spreading ridge or in the oceanic arc was accreted to the front of the arc. These rocks acted as olistostromes enclosed in a Middle Triassic turbiditic sequence in the accretionary prism (Wang et al., 2000a; Faure et al., 2016). The collision then resulted in the emplacement of the ophiolitic mélange and ended in the Triassic, as indicated by regional Permian to Triassic disconformities (BGMRY, 1990).

CONCLUSION

In this study, we focused on two different crustal sequences of the Jinshajiang ophiolite. Based on previous geochronological studies, it is proposed that these two crustal sequences record different stages in development of the Jinshajiang Ocean. The 343 Ma Zhiyong lavas show geochemical affinities to E-MORB, suggesting that they formed in the spreading ridge of the Jinshajiang Ocean. In contrast, the 283 Ma Baimaxueshan lavas and gabbros have volcanic arc–like compositions with depletions in HFSEs and lower Nd isotope ratios, indicating that the Baimaxueshan crustal sequence formed in an oceanic subduction zone. Comparison with the Ailaoshan ophiolite highlights the influence of a mantle plume on the evolution of the Jinshajiang suture zone. Integrating our data with data in the literature, we proposed an evolutionary model of the Jinshajiang-Ailaoshan Ocean from its rifting in the Devonian to final collision between the Qamdo-Simao block and the Yangtze block in the Late Permian–Early Triassic.

ACKNOWLEDGMENTS

We appreciate the assistance of Jing Hu, Yifan Yin, and Xiaobiao Li with trace-element and Sr-Nd isotope measurements at the State Key Laboratory of Ore Deposit Geochemistry, Chinese Academy of Sciences. This study was jointly supported by the National Natural Science Foundation of China (41425011) and the Strategic Priority Research Program (B) of the Chinese Academy of Sciences (XDB18000000). We are grateful to Xiao Wenjiao, Michel Faure, and an anonymous reviewer, and the editor, Damian Nance, who kindly provided constructive comments that greatly improved the quality of the manuscript. We would also like to thank Xiaohu He, Chang Zhang, and Qiwei Li for their suggestions and discussions during the revision of this paper.

REFERENCES CITED

Bender, J.F., Hodges, F.N., and Bence, A.E., 1978, Petrogenesis of basalts from the project FAMOUS area: Experimental study from 0 to 15 kbars: *Earth and Planetary Science*

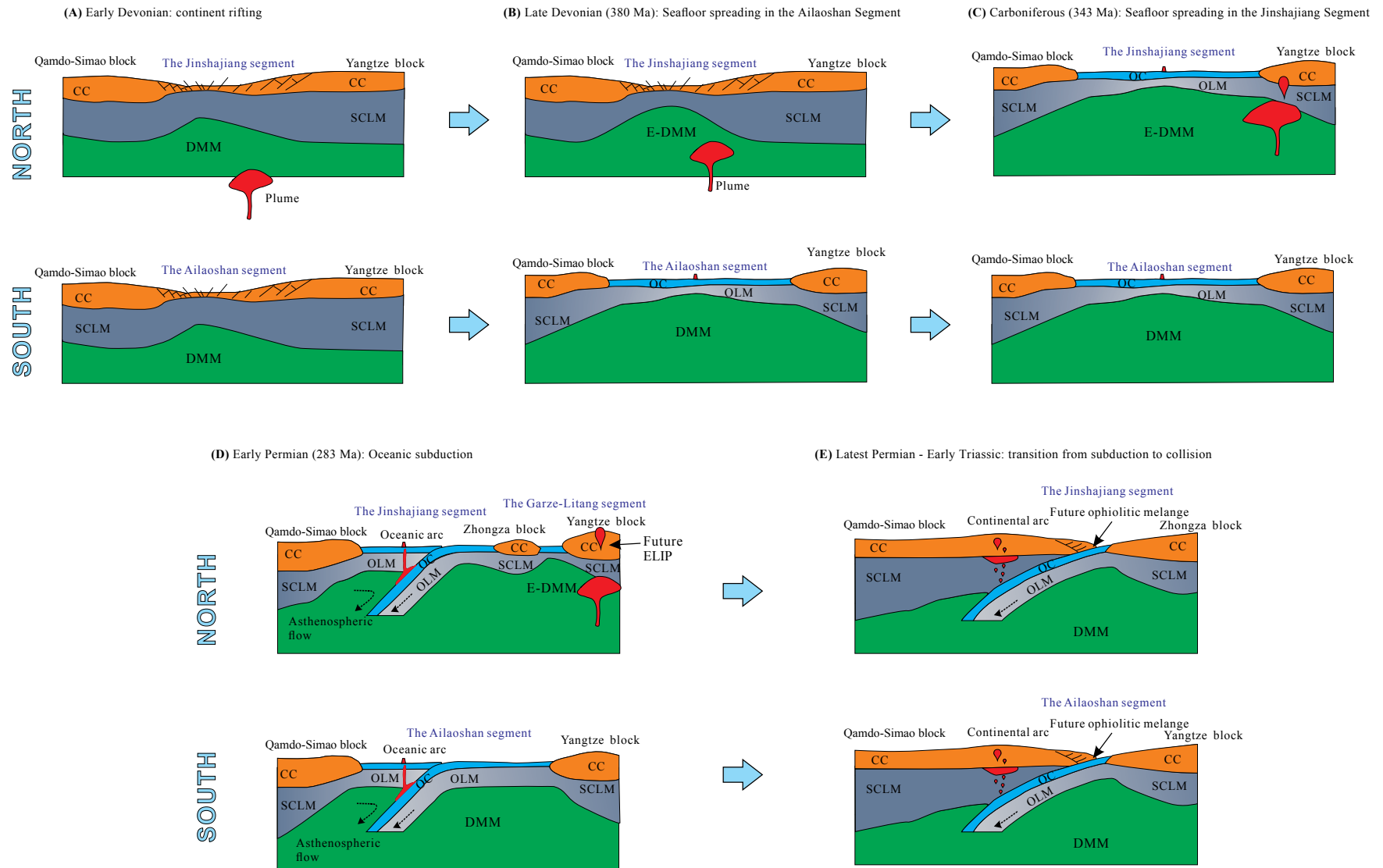


Figure 11. Diagram of the evolutionary stages of the Jinshajiang-Ailaoshan Ocean. (A) Rifting of the Yangtze craton in the Early Devonian. The rifted western Yangtze margin consists of two segments, the Ailaoshan segment in the south and the Jinshajiang segment in the north. (B) In the Late Devonian, the Ailaoshan segment stepped into the seafloor spreading stage, while the Jinshajiang segment remained in the rifting stage. (C) At 340 Ma, deep melt from the mantle plume transformed the established Jinshajiang rift system into a volcanic rift margin. Meanwhile, the asthenosphere in the Jinshajiang segment had been influenced by the plume and therefore could produce oceanic crust comparable to enriched mid-ocean-ridge basalt (E-MORB). (D) The Jinshajiang-Ailaoshan Ocean started to close by westward subduction under the Qamdo-Simao block in the Early Permian. Subduction of the Jinshajiang oceanic lithosphere induced the Zhongza block to separate from the Yangtze block, resulting in opening of the Garze-Litang Ocean along the western Yangtze. The closure of the ocean caused a change in the relative position between the mantle plume and the Yangtze block, which later generated the ca. 260 Ma Emeishan flood basalt (Xiao et al., 2008). (E) Transition from subduction to collision from the Late Permian to the Early Triassic. Abbreviations: CC—continental crust; OC—oceanic crust; DDM—depleted mid-ocean-ridge basalt (MORB) mantle; D-DMM—depleted-DMM; E-DMM—enriched-DMM; SCLM—subcontinental lithospheric mantle; OLM—oceanic lithospheric mantle; ELIP—Emeishan large igneous province.

- Letters, v. 41, p. 277–302, [https://doi.org/10.1016/0012-821X\(78\)90184-X](https://doi.org/10.1016/0012-821X(78)90184-X).
- Bezard, R., Davidson, J.P., Turner, S., Macpherson, C.G., Lindsay, J.M., and Boyce, A.J., 2014, Assimilation of sediments embedded in the oceanic arc crust: Myth or reality?: *Earth and Planetary Science Letters*, v. 395, p. 51–60, <https://doi.org/10.1016/j.epsl.2014.03.038>.
- Brenan, J.M., Shaw, H.F., Ryerson, F.J., and Phinney, D.L., 1995, Mineral-aqueous fluid partitioning of trace elements at 900 C and 2.0 GPa: Constraints on the trace element chemistry of mantle and deep crustal fluids: *Geochimica et Cosmochimica Acta*, v. 59, p. 3331–3350, [https://doi.org/10.1016/0016-7037\(95\)00215-L](https://doi.org/10.1016/0016-7037(95)00215-L).
- Bureau of Geology and Mineral Resources of Sichuan Province (BGMRSP), 1991, Regional Geology of Sichuan Province: Beijing, Geological Publishing House, 728 p. (in Chinese with English abstract).
- Bureau of Geology and Mineral Resources of Yunnan Province (BGMRYP), 1990, Regional Geology of Yunnan Province: Beijing, Geological Publishing House, 728 p. (in Chinese with English abstract).
- Crawford, A.J., Falloon, T.J., and Green, D.H., 1989, Classification, petrogenesis and tectonic setting of boninites, in Crawford, A.J., ed., *Boninites and Related Rocks*: London, Unwin Hyman, p. 1–49.
- Cushman, B., Sinton, J., Ito, G., and Dixon, J.E., 2004, Glass compositions, plume-ridge interaction, and hydrous melting along the Galápagos spreading center, 90.5°W to 98°W: *Geochemistry Geophysics Geosystems*, v. 5, Q08E17, <https://doi.org/10.1029/2004GC000709>.
- Deng, J., Wang, Q., Li, G., Li, C., and Wang, C., 2014, Tethys tectonic evolution and its bearing on the distribution of important mineral deposits in the Sanjiang region, SW China: *Gondwana Research*, v. 26, p. 419–437, <https://doi.org/10.1016/j.gr.2013.08.002>.
- Dilek, Y., and Furnes, H., 2011, Ophiolite genesis and global tectonics: Geochemical and tectonic fingerprinting of ancient oceanic lithosphere: *Geological Society of America Bulletin*, v. 123, p. 387–411, <https://doi.org/10.1130/B30446.1>.
- Dilek, Y., and Furnes, H., 2014, Ophiolites and their origins: *Elements*, v. 10, p. 93–100, <https://doi.org/10.2113/gselements.10.2.93>.
- Falloon, T.J., and Danyushevsky, L.V., 2000, Melting of refractory mantle at 1.5, 2 and 2.5 GPa under anhydrous and H₂O-undersaturated conditions: Implications for the petrogenesis of high-Ca boninites and the influence of subduction components on mantle melting: *Journal of Petrology*, v. 41, p. 257–283, <https://doi.org/10.1093/ptrology/41.2.257>.
- Fan, W., Wang, Y., Zhang, A., Zhang, F., and Zhang, Y., 2010, Permian arc-back-arc basin development along the Ailaoshan tectonic zone: Geochemical, isotopic and geochronological evidence from the Mojiang volcanic rocks, southwest China: *Lithos*, v. 119, p. 553–568, <https://doi.org/10.1016/j.lithos.2010.08.010>.
- Faure, M., Lin, W., Chu, Y., and Lepvrier, C., 2016, Triassic tectonics of the southern margin of the South China block: *Comptes Rendus Geoscience*, v. 348, p. 5–14, <https://doi.org/10.1016/j.crte.2015.06.012>.
- Feng, Q.L., Ge, M.C., Xie, D.F., Ma, Z., and Jiang, Y.S., 1999, Stratigraphic sequence and tectonic evolution in passive continental margin, Jinshajiang belt, northwestern Yunnan Province, China: *Earth Science—Journal of China University of Geosciences*, v. 24, p. 553–557 (in Chinese with English abstract).
- Froitzheim, N., and Manatschal, G., 1996, Kinematics of Jurassic rifting, mantle exhumation, and passive-margin formation in the Austroalpine and Penninic nappes (eastern Switzerland): *Geological Society of America Bulletin*, v. 108, p. 1120–1133, [https://doi.org/10.1130/0016-7606\(1996\)108<1120:KOJRM>2.3.CO;2](https://doi.org/10.1130/0016-7606(1996)108<1120:KOJRM>2.3.CO;2).
- Fujii, T., and Bougault, H., 1983, Melting relations of a magmatic abyssal tholeiite and the origin of MORBs: *Earth and Planetary Science Letters*, v. 62, p. 283–295, [https://doi.org/10.1016/0012-821X\(83\)90091-2](https://doi.org/10.1016/0012-821X(83)90091-2).
- Gaetani, G.A., Grove, T.L., and Bryan, W.B., 1993, The influence of water on the petrogenesis of subduction-related igneous rocks: *Nature*, v. 365, p. 332, <https://doi.org/10.1038/365332a0>.
- Grove, T.L., Gerlach, D.C., and Sando, T.W., 1982, Origin of calc-alkaline series lavas at Medicine Lake volcano by fractionation, assimilation and mixing: *Contributions to Mineralogy and Petrology*, v. 80, p. 160–182, <https://doi.org/10.1007/BF00374893>.
- Hopper, J.R., Funck, T., Tucholke, B.E., Larsen, H.C., Holbrook, W.S., Loudon, K.E., Shillington, D., and Lau, H., 2004, Continental breakup and the onset of ultraslow seafloor spreading off Flemish Cap on the Newfoundland rifted margin: *Geology*, v. 32, p. 93–96, <https://doi.org/10.1130/G19694.1>.
- Hu, W.J., Zhong, H., Zhu, W.G., and He, X.H., 2015, Elemental and Sr-Nd isotopic geochemistry of the basalts and microgabbros in the Shuanggou ophiolite, SW China: Implication for the evolution of the Palaeotethys Ocean: *Geological Magazine*, v. 152, p. 210–224, <https://doi.org/10.1017/S0016756814000259>.
- Ishizuka, O., Tani, K., Reagan, M.K., Kanayama, K., Umino, S., Harigane, Y., Sakamoto, I., Miyajima, Y., Yuasa, M., and Dunkley, D. J., 2011, The timescales of subduction initiation and subsequent evolution of an oceanic island arc: *Earth and Planetary Science Letters*, v. 306, p. 229–240, <https://doi.org/10.1016/j.epsl.2011.04.006>.
- Jahn, B.M., Wu, F.Y., Lo, C.H., and Tsai, C.H., 1999, Crust-mantle interaction induced by deep subduction of the continental crust: Geochemical and Sr-Nd isotopic evidence from post-collisional mafic-ultramafic intrusions of the northern Dabie complex, central China: *Chemical Geology*, v. 157, p. 119–146, [https://doi.org/10.1016/S0009-2541\(98\)00197-1](https://doi.org/10.1016/S0009-2541(98)00197-1).
- Jian, P., Liu, D., and Sun, X., 2008, SHRIMP dating of the Permo-Carboniferous Jinshajiang ophiolite, southwestern China: Geochronological constraints for the evolution of Paleo-Tethys: *Journal of Asian Earth Sciences*, v. 32, p. 371–384, <https://doi.org/10.1016/j.jseaes.2007.11.006>.
- Jian, P., Liu, D., Kröner, A., Zhang, Q., Wang, Y., Sun, X., and Zhang, W., 2009a, Devonian to Permian plate tectonic cycle of the Paleo-Tethys orogen in southwest China (I): Geochemistry of ophiolites, arc/back-arc assemblages and within-plate igneous rocks: *Lithos*, v. 113, p. 748–766, <https://doi.org/10.1016/j.lithos.2009.04.004>.
- Jian, P., Liu, D., Kröner, A., Zhang, Q., Wang, Y., Sun, X., and Zhang, W., 2009b, Devonian to Permian plate tectonic cycle of the Paleo-Tethys orogen in southwest China (II): Insights from zircon ages of ophiolites, arc/back-arc assemblages and within-plate igneous rocks and generation of the Emeishan CFB province: *Lithos*, v. 113, p. 767–784, <https://doi.org/10.1016/j.lithos.2009.04.006>.
- Johnson, M.C., and Plank, T., 2000, Dehydration and melting experiments constrain the fate of subducted sediments: *Geochemistry Geophysics Geosystems*, v. 1, 1007, <https://doi.org/10.1029/1999GC000014>.
- Kessel, R., Schmidt, M.W., Ulmer, P., and Pettke, T., 2005, Trace element signature of subduction-zone fluids, melts and supercritical liquids at 120–180 km depth: *Nature*, v. 437, p. 724–727, <https://doi.org/10.1038/nature03971>.
- Lai, C.K., Meffre, S., Crawford, A.J., Zaw, K., Halpin, J.A., Xue, C.D., and Salam, A., 2014a, The Central Ailaoshan ophiolite and modern analogs: *Gondwana Research*, v. 26, p. 75–88, <https://doi.org/10.1016/j.gr.2013.03.004>.
- Lai, C.K., Meffre, S., Crawford, A.J., Zaw, K., Xue, C.D., and Halpin, J.A., 2014b, The Western Ailaoshan volcanic belts and their SE Asia connection: A new tectonic model for the Eastern Indochina block: *Gondwana Research*, v. 26, p. 52–74, <https://doi.org/10.1016/j.gr.2013.03.003>.
- Leloup, P.H., Lacassin, R., Tapponnier, P., Schärer, U., Zhong, D., Liu, X., Zhang, L., Ji, S., and Trinh, P.T., 1995, The Ailao Shan-Red River shear zone (Yunnan, China), Tertiary transform boundary of Indochina: *Tectonophysics*, v. 251, p. 3–84.
- Le Roux, P.J., Le Roex, A.P., Schilling, J.G., Shimizu, N., Perkins, W.W., and Pearce, N.J.G., 2002, Mantle heterogeneity beneath the southern Mid-Atlantic Ridge: Trace element evidence for contamination of ambient asthenospheric mantle: *Earth and Planetary Science Letters*, v. 203, p. 479–498, [https://doi.org/10.1016/S0012-821X\(02\)00832-4](https://doi.org/10.1016/S0012-821X(02)00832-4).
- Li, G., Li, C., Ripley, E.M., Kamo, S., and Su, S., 2012, Geochronology, petrology and geochemistry of the Nanlinshan and Banpo mafic-ultramafic intrusions: Implications for subduction initiation in the eastern Paleo-Tethys: *Contributions to Mineralogy and Petrology*, v. 164, p. 773–788, <https://doi.org/10.1007/s00410-012-0770-4>.
- Li, W.C., Pan, G.T., Hou, Z.Q., Mo, X.X., Wang, L.Q., and Ding, J., 2010, Metallogenic and Exploration Techniques of Multi-Island-Arc Basin-Collision Orogenic Belt in Southwest the “Three Rivers”: Beijing, Geological Publishing House, 107 p. (in Chinese).
- Li, X., Jiang, X., Sun, Z., Shen, G., and Du, D., 2002, The Collision Orogenic Processes of the Nujiang Lancangjiang-Jinshajiang Area, SW China: Beijing, Geological Publishing House, 213 p. (in Chinese with English abstract).
- McKenzie, D.A.N., and O’Nions, R.K., 1991, Partial melt distributions from inversion of rare earth element concentrations: *Journal of Petrology*, v. 32, p. 1021–1091.
- McKenzie, D.A.N., and O’Nions, R.K., 1995, The source regions of ocean island basalts: *Journal of Petrology*, v. 36, p. 133–159.
- Metcalfe, I., 1996, Gondwanaland dispersion, Asian accretion and evolution of eastern Tethys: *Australian Journal of Earth Sciences*, v. 43, p. 605–623, <https://doi.org/10.1080/08120099608728282>.
- Metcalfe, I., 2006, Palaeozoic and Mesozoic tectonic evolution and palaeogeography of East Asian crustal fragments: The Korean Peninsula in context: *Gondwana Research*, v. 9, p. 24–46, <https://doi.org/10.1016/j.gr.2005.04.002>.
- Metcalfe, I., 2011, Palaeozoic–Mesozoic history of SE Asia, in Hall, R., Cottam, M.A., and Wilson, M.E.J., eds., *The SE Asian Gateway: History and Tectonics of the Australia-Asia Collision: Geological Society [London] Special Publication 355*, p. 7–35, <https://doi.org/10.1144/SP355.2>.
- Metcalfe, I., 2013, Gondwana dispersion and Asian accretion: Tectonic and palaeogeographic evolution of eastern Tethys: *Journal of Asian Earth Sciences*, v. 66, p. 1–33, <https://doi.org/10.1016/j.jseaes.2012.12.020>.
- Miyashiro, A., 1973, The Troodos complex was probably formed in an island arc: *Earth and Planetary Science Letters*, v. 19, p. 218–224, [https://doi.org/10.1016/0012-821X\(73\)90118-0](https://doi.org/10.1016/0012-821X(73)90118-0).
- Mo, X.X., Shen, S.Y., Zhu, Q.W., Xu, T., Wei, Q., Tan, J., and Cheng, H., 1998, Volcanics-Ophiolite and Mineralization of Middle-Southern Part in Sanjiang Area of Southwestern China: Beijing, Geological Publishing House, 128 p. (in Chinese with English abstract).
- Montanini, A., Tribuzio, R., and Vernia, L., 2008, Petrogenesis of basalts and gabbros from an ancient continent-ocean transition (External Liguride ophiolites, Northern Italy): *Lithos*, v. 101, p. 453–479.
- Mou, C., and Wang, L., 2000, The evolution of the volcano-sedimentary basin during the Late Triassic in Deqen, Yunnan: *Journal of Mineralogy and Petrology*, v. 20, p. 23–28 (in Chinese with English abstract).
- Nielsen, S.G., and Marschall, H.R., 2017, Geochemical evidence for mélange melting in global arcs: *Science Advances*, v. 3, no. 4, e1602402, <https://doi.org/10.1126/sciadv.1602402>.
- Niu, Y., Gilmore, T., Mackie, S., Greig, A., and Bach, W., 2002, Mineral chemistry, whole-rock compositions, and petrogenesis of Leg 176 gabbros: Data and discussion, in Natland, J.H., et al., *Proceedings of the Ocean Drilling Program, Scientific Results Volume 176*: College Station, Texas, Ocean Drilling Program, p. 1–60.
- O’Hara, M.J., 1968, The bearing of phase equilibria studies in synthetic and natural systems on the origin and evolution of basic and ultrabasic rocks: *Earth-Science Reviews*, v. 4, p. 69–133, [https://doi.org/10.1016/0012-8252\(68\)90147-5](https://doi.org/10.1016/0012-8252(68)90147-5).
- Pamić, J.A., Tomljenović, B., and Balen, D., 2002, Geodynamic and petrogenetic evolution of Alpine ophiolites from the central and NW Dinarides: An overview: *Lithos*, v. 65, p. 113–142, [https://doi.org/10.1016/S0024-4937\(02\)00162-7](https://doi.org/10.1016/S0024-4937(02)00162-7).
- Pearce, J.A., 2014, Immobile element fingerprinting of ophiolites: *Elements*, v. 10, p. 101–108, <https://doi.org/10.2113/gselements.10.2.101>.
- Pearce, J.A., and Robinson, P.T., 2010, The Troodos ophiolite complex probably formed in a subduction initiation, slab edge setting: *Gondwana Research*, v. 18, p. 60–81, <https://doi.org/10.1016/j.gr.2009.12.003>.
- Peng, T., Wang, Y., Zhao, G., Fan, W., and Peng, B., 2008, Arc-like volcanic rocks from the southern Lancangjiang zone, SW China: Geochronological and geochemical constraints on their petrogenesis and tectonic implications: *Lithos*, v. 102, p. 358–373, <https://doi.org/10.1016/j.lithos.2007.08.012>.
- Plank, T., 2005, Constraints from thorium/lanthanum on sediment recycling at subduction zones and the evolution of the continents: *Journal of Petrology*, v. 46, p. 921–944, <https://doi.org/10.1093/ptrology/egi005>.

- Plank, T., and Langmuir, C. H., 1998, The chemical composition of subducting sediment and its consequences for the crust and mantle: *Chemical geology*, v. 145, p. 325–394.
- Presnall, D.C., Dixon, S.A., Dixon, J.R., O'Donnell, T.H., Brenner, N.L., Schrock, R.L., and Dycus, D.W., 1978, Liquidus phase relations on the join diopside-forsterite-anorthite from 1 atm to 20 kbar: Their bearing on the generation and crystallization of basaltic magma: *Contributions to Mineralogy and Petrology*, v. 66, p. 203–220, <https://doi.org/10.1007/BF00372159>.
- Presnall, D.C., Dixon, J.R., O'Donnell, T.H., and Dycus, S.A., 1979, Generation of mid-ocean ridge tholeiites: *Journal of Petrology*, v. 20, p. 3–35, <https://doi.org/10.1093/ptrology/20.1.3>.
- Qi, L., Hu, J., and Gregoire, D.C., 2000, Determination of trace elements in granites by inductively coupled plasma mass spectrometry: *Talanta*, v. 51, p. 507–513, [https://doi.org/10.1016/S0039-9140\(99\)00318-5](https://doi.org/10.1016/S0039-9140(99)00318-5).
- Reagan, M.K., Ishizuka, O., Stern, R.J., Kelley, K.A., Ohara, Y., Blichert-Toft, J., Bloomer, S.H., Cash, J., Fryer, P., Hanan, B.B., Hickey-Vargas, R., Ishii, T., Kimura, J.-I., Peate, D.W., Rowe, M.C., and Woods, M., 2010, Fore-arc basalts and subduction initiation in the Izu-Bonin-Mariana system: *Geochemistry Geophysics Geosystems*, v. 11, no. 3, Q03X12, <https://doi.org/10.1029/2009GC002871>.
- Schaltegger, U., Desmurs, L., Manatschal, G., Müntener, O., Meier, M., Frank, M., and Bernoulli, D., 2002, The transition from rifting to sea-floor spreading within a magma-poor rifted margin: Field and isotopic constraints: *Terra Nova*, v. 14, p. 156–162.
- Schilling, J.G., 1973, Iceland mantle plume: *Geochemical study of Reykjanes Ridge*: *Nature*, v. 242, p. 565–571, <https://doi.org/10.1038/242565a0>.
- Schilling, J.G., Zajac, M., Evans, R., Johnston, T., White, W., Devine, J.D., and Kingsley, R., 1983, Petrologic and geochemical variations along the Mid-Atlantic Ridge from 29°N to 73°N: *American Journal of Science*, v. 283, p. 510–586, <https://doi.org/10.2475/ajs.283.6.510>.
- Şengör, A.M.C., 1987, Tectonics of the Tethysides—Orogenic collage development in a collisional setting: *Annual Review of Earth and Planetary Sciences*, v. 15, p. 213–244, <https://doi.org/10.1146/annurev.ea.15.050187.001241>.
- Shaw, D.M., 1970, Trace element fractionation during anatexis: *Geochimica et Cosmochimica Acta*, v. 34, p. 237–243, [https://doi.org/10.1016/0016-7037\(70\)90009-8](https://doi.org/10.1016/0016-7037(70)90009-8).
- Stampfli, G.M., and Borel, G.D., 2002, A plate tectonic model for the Paleozoic and Mesozoic constrained by dynamic plate boundaries and restored synthetic oceanic isochrons: *Earth and Planetary Science Letters*, v. 196, no. 1–2, p. 17–33, [https://doi.org/10.1016/S0012-821X\(01\)00588-X](https://doi.org/10.1016/S0012-821X(01)00588-X).
- Sun, S.S., and McDonough, W.F., 1989, Chemical and isotopic systematics of oceanic basalts: Implications for mantle composition and processes, *in* Saunders, A.D., and Norry, M.J., eds., *Magmatism in the Ocean Basins*: Geological Society [London] Special Publication 42, p. 313–345, <https://doi.org/10.1144/GSL.SP.1989.042.01.19>.
- Sun, X., and Jian, P., 2004, The Wilson cycle of the Jinshajiang Paleo-Tethys Ocean, in western Yunnan and Sichuan Provinces: *Geological Review (Dizhi Lunping)*, v. 50, p. 343–350 (in Chinese with English abstract).
- Tan, F., 2002, The sedimentary characteristics of Simao Triassic rear arc foreland basin, Yunnan Province: *Acta Sedimentologica Sinica*, v. 20, p. 560–567 (in Chinese with English abstract).
- Tatsumi, Y., and Maruyama, S., 1989, Boninites and high-Mg andesites: Tectonics and petrogenesis, *in* Crawford, A.J., ed., *Boninites and Related Rocks*: London, Unwin Hyman, p. 50–71.
- Taylor, R.N., Nesbitt, R.W., Vidal, P., Harmon, R.S., Austruy, B., and Croudace, I.W., 1994, Mineralogy, chemistry, and genesis of the boninite series volcanics, Chichijima, Bonin Islands, Japan: *Journal of Petrology*, v. 35, p. 577–617, <https://doi.org/10.1093/ptrology/35.3.577>.
- Wang, P., 1985, Petrochemistry of the ophiolite-associated lavas in Deqin, Yunnan: *Contribution of the Geology of the Qinhai-Xizang (Tibet) Plateau*, v. 9, p. 207–219 (in Chinese with English abstract).
- Wang, X., Metcalfe, I., Jian, P., He, L., and Wang, C., 2000a, The Jinshajiang–Ailaoshan suture zone, China: Tectonostratigraphy, age and evolution: *Journal of Asian Earth Sciences*, v. 18, p. 675–690, [https://doi.org/10.1016/S1367-9120\(00\)00039-0](https://doi.org/10.1016/S1367-9120(00)00039-0).
- Wang, Y., Li, X., Duan, L., Huang, Z., and Chui, C., 2000b, Geotectonics and Metallogeny in South Nuijiang–Langchang–Jinsha Rivers Area: Beijing, Geological Publishing House, 123 p. (in Chinese with English abstract).
- Wang, Y., Fan, W., Zhang, Y., Peng, T., Chen, X., and Xu, Y., 2006, Kinematics and ⁴⁰Ar/³⁹Ar geochronology of the Gaoligong and Chongshan shear systems, western Yunnan, China: Implications for early Oligocene tectonic extrusion of SE Asia: *Tectonophysics*, v. 418, p. 235–254, <https://doi.org/10.1016/j.tecto.2006.02.005>.
- Wang, Y.J., Qian, X., Cawood, P.A., Liu, H.C., Feng, Q.L., Zhao, G.C., Zhang, Y.H., He, H.Y., and Zhang, P.Z., 2018, Closure of the East Paleotethyan Ocean and amalgamation of the Eastern Cimmerian and Southeast Asia continental fragment: *Earth-Science Reviews*, v. 186, p. 195–230, <https://doi.org/10.1016/j.earscirev.2017.09.013>.
- Wei, G.Y., Feng, G.R., Luo, Z.W., Wu, S.Z., and Tao, Y.Y., 1984, Stratigraphic sequences of the Lancang and Chongshan groups in western Yunnan and their volcanism and metamorphism: *Journal of Chengdu College of Geology*, v. 2, p. 12–20 (in Chinese with English abstract).
- Whattam, S.A., and Stern, R.J., 2011, The 'subduction initiation rule': A key for linking ophiolites, intra-oceanic forearcs, and subduction initiation: *Contributions to Mineralogy and Petrology*, v. 162, p. 1031–1045, <https://doi.org/10.1007/s00410-011-0638-z>.
- Woelki, D., Regelous, M., Haase, K.M., Romer, R.H.W., and Beier, C., 2018, Petrogenesis of boninitic lavas from the Troodos Ophiolite, and comparison with Izu–Bonin–Mariana fore-arc crust: *Earth and Planetary Science Letters*, v. 498, p. 203–214.
- Workman, R.K., and Hart, S.R., 2005, Major and trace element composition of the depleted MORB mantle (DMM): *Earth and Planetary Science Letters*, v. 231, p. 53–72, <https://doi.org/10.1016/j.epsl.2004.12.005>.
- Wu, S.Z., Tao, Y.Y., Feng, G.R., Wei, G.Y., and Luo, Z.W., 1984, Metavolcanics in the Langchang Group and the Chongshan Group: *Yunnan Geology*, v. 3, p. 113–123 (in Chinese).
- Xiao, L., He, Q., Pirajno, F., Ni, P., Du, J., and Wei, Q., 2008, Possible correlation between a mantle plume and the evolution of Paleo-Tethys Jinshajiang Ocean: Evidence from a volcanic rifted margin in the Xiaru-Tuoding area, Yunnan, SW China: *Lithos*, v. 100, p. 112–126, <https://doi.org/10.1016/j.lithos.2007.06.020>.
- Xu, J.F., and Castillo, P.R., 2004, Geochemical and Nd-Pb isotopic characteristics of the Tethyan asthenosphere: Implications for the origin of the Indian Ocean mantle domain: *Tectonophysics*, v. 393, p. 9–27, <https://doi.org/10.1016/j.tecto.2004.07.028>.
- Yan, Q.R., Wang, Z.Q., Liu, S.W., Li, Q.G., Zhang, H.Y., Wang, T., Liu, D.Y., Shi, Y.R., Jian, P., Wang, J.G., Zhang, D.H., and Zhao, J., 2005, Opening of Tethys in southwest China and its significance to the breakup of East Gondwanaland in the late Paleozoic, evidence from SHRIMP U-Pb zircon analyses for the Garzê ophiolite block: *Chinese Science Bulletin*, v. 50, p. 256–264.
- Yang, K.H., Mo, X.X., and Zhu, Q.W., 1994, Tectono-volcanic belts and late Paleozoic–early Mesozoic evolution of southwestern Yunnan, China: *Journal of Southeast Asian Earth Sciences*, v. 10, p. 245–262, [https://doi.org/10.1016/0743-9547\(94\)90024-8](https://doi.org/10.1016/0743-9547(94)90024-8).
- Yu, Q., Mou, C., and Wang, J., 2000, Sedimentary facies and palaeogeographic evolution of the Lanping Basin in Yunnan: *Sedimentary Geology and Tethyan Geology*, v. 20, p. 33–42 (in Chinese with English abstract).
- Yumul, G.P., Jr., Zhou, M.F., Wang, C.Y., Zhao, T.P., and Dimantlanta, C.B., 2008, Geology and geochemistry of the Shuanggou ophiolite (Ailao Shan ophiolitic belt), Yunnan Province, SW China: Evidence for a slow-spreading oceanic basin origin: *Journal of Asian Earth Sciences*, v. 32, p. 385–395, <https://doi.org/10.1016/j.jseas.2007.11.007>.
- Zhang, Q., Zhou, D. and Li, X., 1995, Characteristics and genesis of Shuanggou ophiolites, Yunnan Province: *Acta Petrologica Sinica*, v. 11, p. 190–202 (in Chinese with English abstract).
- Zhang, Q., Zhou, D., and Zhao, D., 1996, Wilson cycle of the Paleo-Tethyan orogenic belt in western Yunnan: record of magmatism and discussion on mantle processes: *Acta Petrologica Sinica*, v. 12, p. 17–28 (in Chinese with English abstract).
- Zhong, D., 1998, Paleo-Tethyan Orogenic Belt in Western Yunnan and Sichuan: Beijing, Science Press, 231 p. (in Chinese).
- Zi, J.W., Cawood, P.A., Fan, W.M., Tohver, E., Wang, Y.J., and McCuaig, T.C., 2012a, Generation of early Indosinian enriched mantle-derived granitoid pluton in the Sanjiang orogen (SW China) in response to closure of the Paleo-Tethys: *Lithos*, v. 140, p. 166–182, <https://doi.org/10.1016/j.lithos.2012.02.006>.
- Zi, J.W., Cawood, P.A., Fan, W.M., Wang, Y.J., and Tohver, E., 2012b, Contrasting rift and subduction-related plagiogranites in the Jinshajiang ophiolitic mélange, southwest China, and implications for the Paleo-Tethys: *Tectonics*, v. 31, TC2012, <https://doi.org/10.1029/2011TC002937>.
- Zi, J.W., Cawood, P.A., Fan, W.M., Wang, Y.J., Tohver, E., McCuaig, T.C., and Peng, T.P., 2012c, Triassic collision in the Paleo-Tethys Ocean constrained by volcanic activity in SW China: *Lithos*, v. 144, p. 145–160, <https://doi.org/10.1016/j.lithos.2012.04.020>.
- Zi, J.W., Cawood, P.A., Fan, W.M., Tohver, E., Wang, Y.J., McCuaig, T.C., and Peng, T.P., 2013, Late Permian–Triassic magmatic evolution in the Jinshajiang orogenic belt, SW China, and implications for orogenic processes following closure of the Paleo-Tethys: *American Journal of Science*, v. 313, p. 81–112, <https://doi.org/10.2475/02.2013.02>.

MANUSCRIPT RECEIVED 7 APRIL 2019

REVISED MANUSCRIPT RECEIVED 12 AUGUST 2019

MANUSCRIPT ACCEPTED 18 SEPTEMBER 2019